Spring 5-18-2012

Improved operational limits for offshore pipelay vessels

Daniel Rey Givan
dgivan@uno.edu

Improved operational limits for offshore pipelay vessels

A Thesis

Submitted to the Graduate Faculty of the
University of New Orleans
in partial fulfillment of the
requirements for the degree of

Master of Science in Engineering
with a concentration in
Naval Architecture & Marine Engineering

by

Daniel R. Givan

B.S. University of New Orleans, 2010

May, 2012

Acknowledgement

I am grateful to Dr. Brandon Taravella, my thesis advisor. His direction and feedback made it possible for me to complete this thesis and inspired me to continue my education in this field. I would also like to thank Dr. Lothar Birk for serving on my thesis committee and providing invaluable teaching in this field. I am appreciative of their sound teaching and advice throughout my undergraduate and graduate studies at the University of New Orleans. Dr. Nikolaos Xiros should be thanked for his willingness to serve on my thesis committee in the last months and for his input to this project.

I wish to thank Mr. Raymond Serpas with McDermott, Inc. for his technical guidance on pipelay operations and for allowing the usage of *MOSES* on this academic work.

Last but not least, I would like to thank my wife, Kallyn, for her support, encouragement, understanding, and patience throughout the process of completing my graduate degree.

Nomenclature

A	Projected pipeline area
b	Damping parameter
C_a	Added mass coefficient
C_d	Drag coefficient
C_m	Hydrodynamic mass coefficient
d_0	Water depth, same as *WD*
dF_m	Differential drag force (Morison)
D	Pipe diameter
E	Young's modulus
EI	Flexural rigidity of steel pipe
F_s	Effective tension force
$F_{S_{st}}$	Static component of the effective tension force
$F_{S_{dy}}$	Dynamic component of the effective tension force
g	Gravitational acceleration = 9.81 m/s^2
H_s	Significant wave height
I	Moment of inertia
k	On the sea bottom: pipe subgrade modulus, in the free span: zero
KC	Keuligan Carpenter number
L	Unsupported length
M_T	Torque
m	Mass per length of the pipeline
m_0	Variance of wave spectrum, zeroth order moment
m_1	First order moment
P	Pressure
q_N	Distributed load on pipeline not due to motion in the static plane
q_B	Distributed load on pipeline not due to motion perpendicular to the static plane
s	Curve length from the touch-down point, positive upwards
S_R	Response spectrum
S_ζ	Sea spectrum
$S_{\sigma_{DYN}}$	Dynamic stress response spectrum

T	Period
T_m	Mean wave period
t	Time
t_s	Steel wall thickness of pipe
u_N	Dynamic bending deflections in the static plane
u_B	Dynamic bending deflections perpendicular to the static plane
u_{Sv}	Vessel motion component tangential to the pipe
Δu_S	Axial pipe motion relative to the vessel
V	Water particle velocity
v_N	External flow velocity lateral to the pipe in the static plane
v_B	External flow velocity lateral to the pipe perpendicular to the static plane
WL	Wave length
z	Depth
∇	Gradient
ε	Strain
υ	Poisson's ratio
ω	Frequency
ω_e	Encounter frequency
ϕ	Velocity potential
φ	Static inclination angle of pipeline
φ'	Static curvature of pipeline
ρ	Specific mass of sea water = 1025 kg/m^3
σ_φ	Circumferential pipe stress
σ_S	Bending pipe stresses
σ_{eq}	Equivalent pipe stress
ζ_a	Wave amplitude
$\{\}'$	Derivative along pipe length, $\frac{\partial}{\partial s}$
$\dot{\{\}}$	Derivative on time, $\frac{\partial}{\partial t}$

Table of Contents

List of Figures

List of Tables

Abstract

Subsea pipelines are used extensively throughout the world's oceans to transport oil and gas from offshore facilities to land, often hundreds of miles. These pipelines range in diameter from three to sixty inches and are installed in deeper depths every year, currently as deep as 2,900 meters. Pipeline construction and installation costs are a large percentage of offshore projects and thus, methods toward reducing costs is an imperative objective. With pipeline installation projects taking place in harsher environments, vessel operability is vital. This work presents an improved method for determining limiting criteria for pipelay operations to more effectively plan and execute offshore projects. This improvement is based on the consideration of total effective pipeline stresses as the limiting criterion rather than the traditionally used limiting pitch angle. Limiting sea curves based on a sample dynamic pipeline analysis are shown and their incorporation in workability planning is discussed.

Keywords: Pipelay, Pipeline Installation, Offshore Construction, Hydrodynamics, Workability

Section 1 - Introduction

1.1. Background

The offshore construction industry has progressed rapidly in the last 30 years as the World's increased demand for petroleum products has necessitated the exploration of deeper water. Today, subsea oil fields are being constructed in water depths of nearly 3,000 meters due to large advancements in subsea equipment and the vessels which install it. At depths of this magnitude, the ocean presents challenges not existing closer to the surface, including drift currents, temperature changes, and extreme terrain.

Purpose-built vessels have been constructed for the use of installing pipelines and are catered to a specific component of subsea construction, such as rigid pipelines, flexible flowlines, umbilicals, or data communication cables. Designs have progressed from flat-bottom deck barges equipped with a truss-type stinger to large semisubmersible hulls with adjustable towers to construct deeper offshore. As the industry progressed into harsher environments, a need became apparent for either optimized hull forms or more advanced lay systems, both of which have been the subject of much research over the last few decades.

Today, offshore construction vessels are equipped with bilge keels, anti-roll tanks, motion-suppression tanks, mooring lines, and heave compensation devices to help reduce the movement of suspended pipe loads. However, the addition of these new variables into the modeling of ship dynamics makes it increasingly difficult to make accurate estimates for project planning.

Traditionally, offshore pipelay operations have been restricted based on prevailing environmental conditions, such as the significant wave height, H_S, and mean wave period, T_M. However, these restrictions are generated using idealized wave conditions (single-peak wave spectrum) and vessel Response Amplitude Operators (RAOs) which may be over or under-estimated. Great inaccuracy exists, specifically in roll where non-linear damping makes it

difficult to calibrate a hydrodynamic model. Most offshore environments are not correctly analyzed using these RAOs, particularly where the ocean environment is multidirectional in sea and swell which is often the case in areas offshore West Africa and Brazil [9].

This thesis extends previous efforts to utilize real-time weather data to make improved assessments as to the specific capability of a pipelay vessel. This is done by deriving an analytical method for computing an "instantaneous" response spectrum of a dynamic multi-body system (vessel, stinger, and pipeline) and using it to make more accurate predictions about specific pipelay operations using a dynamic perspective.

1.2. Previous Work

Two types of pipeline analysis exist: static and dynamic. A static pipeline installation analysis checks the pipe laying vessel and the capabilities of its equipment. It is used to set the stinger departure angle, roller heights, initial tension, and determine stresses/strains within the pipe. A dynamic pipeline analysis accounts for vessel dynamics along with wave and current action on the suspended pipeline. Clauss et al. [1] introduced a numerical procedure for analyzing the dynamic stresses in offshore pipelines introduced by a complex ocean environment. Previously, only static analyses had been considered. This procedure was later extended to the determination of limiting sea states for pipeline operations using hydrodynamic modeling software. The results of this analysis dictate in what environment a pipeline can be safely installed. Without this data, offshore projects rely on the judgment of the vessel superintendent who works for the contractor and therefore may have reasons other than pipeline stresses affecting his judgment on whether or not to lay down a pipeline.

In addition, the stochastic ocean environment is impossible to predict and thus, naval architects must make assumptions to provide any realistic approximation of an offshore model. Typically, this involves the use of weather reports of a target area recorded from several

preceding years or decades. A vessel model can be analyzed in the proposed environment and estimates of the ship's motion are made. By setting some basic operating criteria such as limiting the vessel pitch to 1.5 degrees single-amplitude in a 3-hour time window, the vessel operator may have an idea of how one ship can perform a task compared with another. Workability analysis is a useful tool in *comparing* two vessels performing the same operation in identical environments, but is rather poor in estimating how often a ship can work in a short time window.

As many vessels began carrying Motion Recording Units (MRU) as part of dynamic positioning (DP) systems, classification society, Det Norske Veritas, (DNV), began to allow for the use of real time weather data in the execution of marine operations [4]. Legras and Wang [9] proposed that the use of real-time measurement of vessel motion could be used to improve the determination of limiting criteria in offshore crane operations. Using the MRU data, they proposed that more accurate RAOs could be generated for the lifted object than using office-based hydrodynamics software operating under numerous assumptions. The usage of real-time ship motion data alleviates these concerns as all variables are captured at a given instant. Legras and Wang focused only on a single degree of freedom, heave, and lacked an analytical method for computing added mass and damping coefficients of subsea equipment.

Valen [14] investigated the operational limits further using DNV Recommended Practices [4] and an industry standard hydrodynamics software. He noted that performing time domain simulations based on real-time data can increase operational limits but are still limited by inaccuracies in the added mass and damping of the lifted equipment as well as external factors, such as extreme forecasts, scheduling, or equipment malfunctions. Expanding this methodology to pipelay analysis is not illogical. Clauss et al. [3] concluded that "a real-time pipe stress

analysis based on measured vessel motions during the pipe laying process seems to be a feasible application."

1.3. Proposed Work

This work presents a new method for determining limiting criteria for pipelay operations to more effectively plan and execute these projects in the dynamic ocean environment. This improvement is based on the use of real time wave elevation data along with modeling of the hydrodynamic effects involved in a pipelaying operation. Results using a commercially available hydrodynamics software suite are presented and used within a program to compute the timely operational limits.

Section 2 – Problem Setup

2.1. Ideal Flow Theory

The use of ideal flow theory to investigate sea keeping can provide quick, qualitative understanding of a system compared with detailed testing at the model scale or solving the Reynold's Averaged Navier-Stokes (RANS) equations in a Computational Fluid Dynamics (CFD) solver. Commercially available ideal flow solvers provide accurate estimates for most linear systems.

The common assumptions made in ideal flow theory are that the fluid is incompressible, irrotational, and inviscid, and that the conservation of mass is not violated. These assumptions are not all that unreasonable, but the boundary layer of a ship does contain viscosity.

Using the Divergence Theorem, the continuity equation for an incompressible (constant-density) fluid is:

$$\vec{\nabla} \cdot \vec{V} = 0 \tag{1}$$

where $\vec{\nabla}$ is the divergence. The equation states that the flux of matter across a volume boundary is equal to the generation of matter within the volume. A fluid without particle rotation is:

$$\vec{V} = \vec{\nabla}\phi \tag{2}$$

where ϕ is the unknown scalar velocity potential which is to be solved. An irrotational fluid is also inviscid by nature.

Substituting (2) into (1) gives the well-known Laplace equation.

$$\vec{\nabla}^2\phi = 0 \tag{3}$$

which is a linear second-order partial differential equation.

From (3), Bernoulli's equation provides pressures if the velocities and potentials are known.

$$\frac{P}{\rho} + \frac{\partial\phi}{\partial t} + \frac{1}{2}\left|\vec{V}^2\right| + gz = 0 \tag{4}$$

The velocity potential, ϕ, is found by satisfying the boundary conditions, and the velocities by taking its gradient. Then, once the pressure, *P*, is computed from (4), the hydrodynamic forces are found by integrating over the body's surface in the direction of interest [12]. Hydrodynamic software packages, such as *WAMIT*, *MOSES*, and *Octopus* have built-in solvers for these forces based on 2-D strip theory or 3-D diffraction/panel methods.

Ship motions can be characterized using a transfer function which normalizes the response by a wave with unit amplitude. From the linear assumption, these Response Amplitude Operators provide a basis by which comparisons can be made from one system to another.

$$RAO(\omega_e) = \frac{X(\omega_e)}{\zeta_a} \tag{5}$$

where $X(\omega_e)$ is the system response for a particular frequency of encounter.

The set of motion RAOs, six in all, describe the system motion for each degree of freedom (DOF): surge, sway, heave, roll, pitch, and yaw. The function, by nature, incorporates external factors, including restoring forces and moments, added mass, and damping. It represents the response of a system to a unit excitation. Beyond motion, transfer functions can be used to represent any physical property, including dynamic pipeline stress and are determined in a similar fashion to motion RAOs.

2.2. Sea Spectra Derivation

Irregular ocean seas can be modeled using a series of superimposed regular sinusoidal waves which, combined, contain a specific amount of energy based on height and frequency. The amount of energy in a single sinusoidal wave is:

$$E = \frac{1}{2}\rho g {\zeta_a}^2 \tag{6}$$

Summing all of the waves gives the total energy in a unit area:

$$E_T = \frac{1}{2}\rho g \sum_{i=1}^{N} {\zeta_a}^2 \tag{7}$$

An energy density spectrum is the frequency distribution of energy for a particular environment and typically takes the shape of a Rayleigh distribution. Significant research has produced a set of well recognized spectra characterized by height and frequency. Some of these are the ISSC, Bretschneider, JONSWAP, and Pierson-Moskowitz spectra. These functions are empirical in nature but closely resemble target environments stemming from decades of observation. For example, the ISSC spectrum is defined as:

$$S(\omega) = \frac{173{H_s}^2}{{T_m}^4\omega^5} e^{\left(-691/(\omega T_m)^4\right)} \tag{8}$$

While these functions can be shown to be good tools for predicting a system's response in a specific environment, this work will focus on using *real-time data* to derive an energy density spectrum to more accurately analyze the system in its current environment.

To create an estimate of the energy density spectrum from a time series of wave data, a wave probe is dropped near the vessel and its motion is recorded. A spectrum can be computed using a Fast Fourier Transform (FFT) of the time series. In theory, the transform is done for an infinitely long time series.

$$S_{\zeta\zeta}(\omega) = \frac{2\$_{\zeta\zeta}(f)}{2\pi} = \frac{2}{2\pi}\lim_{T\to\infty}\frac{1}{T}|F_x(f)|^2 \tag{9}$$

However, in reality an infinite time series is not practical so the energy density spectrum is approximated as below.

$$S_{\zeta\zeta}(\omega) \approx \frac{1}{\pi T}|F_x(f)|^2 \tag{10}$$

In addition to the inaccuracy arising from a discrete time sample, the Fourier transform in (10) is only an approximation of the Fourier integral. Subsequently, the energy density spectrum derived from a time series can look a bit ragged with some frequencies containing significantly different energy than those adjacent to it.

To achieve a more "Rayleigh-type" distribution, the spectrum can be smoothed by splitting the full time series into equal length subsections, estimating the spectrum for each, and then averaging them together. Other, more advanced mathematical methods of smoothing are available. For example, the Hanning window method using raised cosine filters with overlapping windows rather than adjacent samples [13]. With $2m-1$ windows overlapping to the midpoints, the cosine filter is applied:

$$u(t) = \sqrt{\frac{8}{3}} * \left(1 - cos^2\left(\frac{\pi t}{T}\right)\right) \tag{11}$$

The FFT is then performed on each time window with signal $\zeta(t)u(t)$ and the results for all windows are averaged to create the final smoothed spectrum.

2.3. Statistical Properties of a Spectrum

Statistics of a spectrum are computed to determine various properties of the environment which are valid by assuming that a Rayleigh probability distribution exists. The average of the $1/n^{th}$ highest amplitudes can be derived as:

$$A_{1/n} = \sqrt{2m_0}\left\{\sqrt{Ln(n)} + \frac{n\sqrt{\pi}}{2}\left[1 - erf\left(\sqrt{Ln(n)}\right)\right]\right\} \tag{12}$$

From (12), the significant, $1/3^{rd}$ highest wave amplitude can be found:

$$A_{1/3} = 2.00\sqrt{m_0} \tag{13}$$

where m_0 is the variance of the process and the area under the spectral density curve found through integration over frequency, ω.

$$m_0 = \int_0^\infty S_\zeta(\omega)d\omega \tag{14}$$

Higher order spectral moments can be found by adding an additional term to (14).

$$m_n = \int_0^\infty S_\zeta(\omega)\omega^n d\omega \tag{15}$$

Of course, the wave height is the double amplitude and thus, the significant wave height is:

$$H_{1/3} = 4.00\sqrt{m_0} \tag{16}$$

Of interest in this work are statistics over a 72-hour time window, the maximum span of forecast review permitted by DNV [4]. Assuming a low mean wave period of 5 seconds, about 50,000 waves would pass a global point in 72 hours. It is subsequently useful to define the 1/50,000th multiplier as:

$$A_{1/50,000} = 4.652\sqrt{m_0} \tag{17}$$

The mean period of the spectrum is found using the spectral moments:

$$T_M = 2\pi\frac{m_0(\omega)}{m_1(\omega)} \tag{18}$$

As always, the standard conversion between period and frequency is:

$$\omega = \frac{2\pi}{T} \tag{19}$$

Statistics based on a Rayleigh distribution are strictly only valid if a single crest and trough exist between each zero up-crossing point. While not entirely unreasonable, actual environments rarely contain this property exactly. If the spectrum is broader or narrower, the results can be scaled as in Michel [10]. A spectral broadness parameter can be defined as:

$$\varepsilon = \sqrt{1 - \frac{{m_2}^2}{m_0 m_4}} \tag{20}$$

Then, the multipliers from (12) can be corrected:

$$A_{1/n,corrected} = A_{1/n} \cdot \sqrt{1 - \frac{\varepsilon^2}{2}} \tag{21}$$

2.4. System Response Spectra

The response spectrum is then generated by multiplying the square of the RAO by the energy density spectrum. The response spectrum describes how the system behaves in the specific environment described by the wave energy density spectrum.

$$S_R(\omega) = [RAO(\omega)]^2 \cdot S(\omega) \tag{22}$$

Equation (22) follows the same statistical laws as the wave spectrum. Typically, specific motions are of interest in offshore pipelay operations such as the maximum, $1/1000^{th}$, pitch. Excessive pitch angle causes the pipe profile to change, increasing bending stresses in the pipeline. If these stresses exceed certain allowable limits, the pipeline can fail requiring removal and re-installation or underwater repair, both costly events. Thus, offshore contractors closely monitor the vessel motion and cease operations when pre-defined limits are exceeded.

Because pipelay operations take place at relatively slow speeds, this work will not consider the effects of forward speed on encounter frequency. However, it is not unreasonable to expand this method to include forward speed for operations such as flexible cable deployment where forward speed may be non-negligible.

The same method for estimating the energy density spectrum for an environment as in (10) can be used with vessel motion data to derive the ship response energy density spectrum. This is preferred over using wave data and theoretically computed RAOs due to the full capture of all hydrodynamic effects including added mass, damping, and mooring line forces. Using a motion recording unit (MRU) installed onboard primarily for use in dynamic positioning systems, vessel motions can be recorded in real-time and converted to a vessel response spectrum through a Fourier transform. This can likewise be done for pipe stresses if time series data from a pipeline or roller load sensor is available. With a real-time capture of the response spectrum, more accurate predictions can be made into the dynamics of an object suspended from a moving vessel such as a pipeline or subsea equipment unit. Legras and Wang [9] discuss this method in greater detail. Unfortunately, response data for pipeline stress is not as readily available as time series weather data from buoys and therefore, this work will focus on using wave data applied to the hydrodynamic model.

2.5. Pipeline Stress

Offshore pipelines have specific criteria which must be considered during their installation, primarily bending and axial stress limits. If pre-determined values are exceeded, the pipeline can fail, causing extensive underwater repair operations. Significant research has been published on dynamic bending stresses in offshore pipelines, namely by G.F. Clauss et al. [1, 2, 3]. Their work considered, for the first time, the dynamic effects encountered by laying pipelines using a moving foundation. Previously, all analysis had considered only static stresses of a rod element. Their research [2] considered the complex manner in which the lay vessel, stinger, and pipe interact with each other in the ocean environment and produced a method for determining limiting sea states. To proceed, the system is briefly described.

Offshore pipelines are utilized extensively throughout the world to transport oil and gas products to be refined at onshore facilities. Sections of steel pipe are welded together onboard the lay vessel one-by-one, through a series of welding and coating stations. Toward the exit point from the ship, a tension device grips the pipeline to prevent it from buckling under its own weight as it is suspended from the ship to the seabed. This tension also serves to reduce bending in the sag-bend region, that closest to the sea bed. To reduce bending stresses near the top of the pipeline (overbend), two lay methods are used: S-lay and J-lay. Typically, S-lay is used in shallower water (less than about 300 meters) where J-lay is used in deeper water. The difference lies in the shape the pipe creates as it is paid-out from the ship. S-Lay is relatively parallel to the water surface at the stern and is supported by a fixed or articulated stinger. J-Lay is much closer to perpendicular to the water surface at departure which effectively eliminates the over-bend stresses near the top of the pipe although requires substantially more tension to support the pipe. Figures 1 and 2 show a sample of both configurations (Source: Lee [8]).

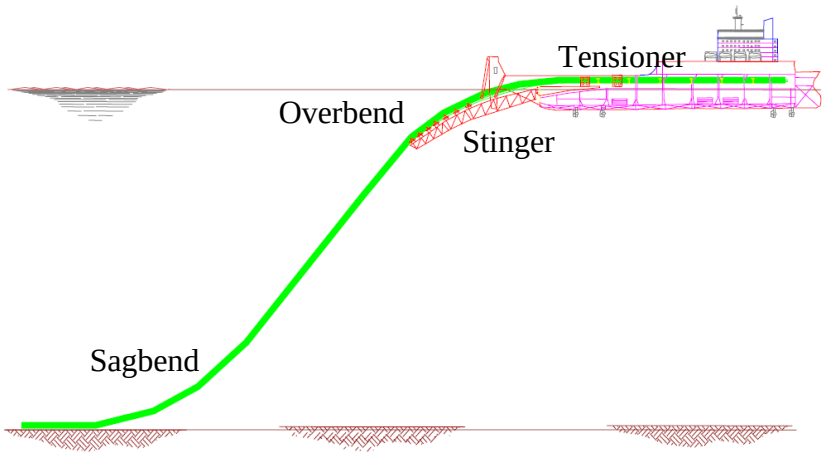

Figure 1: S-Lay Configuration

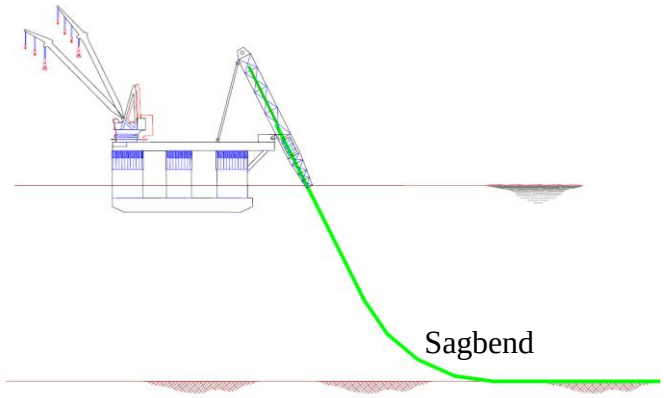

Figure 2: J-Lay Configuration

Clauss et al. [2] expanded on their previous work to incorporate more realistic boundary conditions to capture the oscillations in the pipe and the effects of rollers and tensioners supporting the pipe on the ship. It was proposed that the dynamic analysis of pipelay is based on two differential equations for lateral deflections and one relation between the tension force oscillations and the motion of the tension machine.

$$EIu_N'''' - \left(\left(F_{S_{st}} + F_{S_{dy}}\right)u_N'\right)' + ku_N + b\dot{u}_N + m\ddot{u}_N = q_N + \varphi' F_{S_{dy}} \tag{23}$$

$$EIu_B'''' - \left(\left(F_{S_{st}} + F_{S_{dy}}\right)u_B'\right)' + ku_B + b\dot{u}_B + m\ddot{u}_B = q_B + (\varphi' M_T)' \tag{24}$$

$$\Delta u_S = \frac{L}{EA} F_{S_{dy}} - u_{Sv} + \int_{(L)} \left(\varphi' u_N - \frac{{u_N'}^2 + {u_B'}^2}{2}\right) ds \tag{25}$$

This set of equations has some particular values of interest, such as $F_{S_{st}}$, the static tension force and $\varphi(s)$ which is the pipeline angle at each location, *s*. $F_{S_{dy}}$is the *dynamic tension force* obtained from averaging the tensile equation (25) over the unsupported span, *L*:

$$F_{S_{dy}} = EA\left(u_S' - \varphi' u_N + \left(\frac{{u_N'}^2 + {u_B'}^2}{2}\right)\right) \tag{26}$$

Figure 3 presents the problem setup and coordinate system from Clauss et al [2].

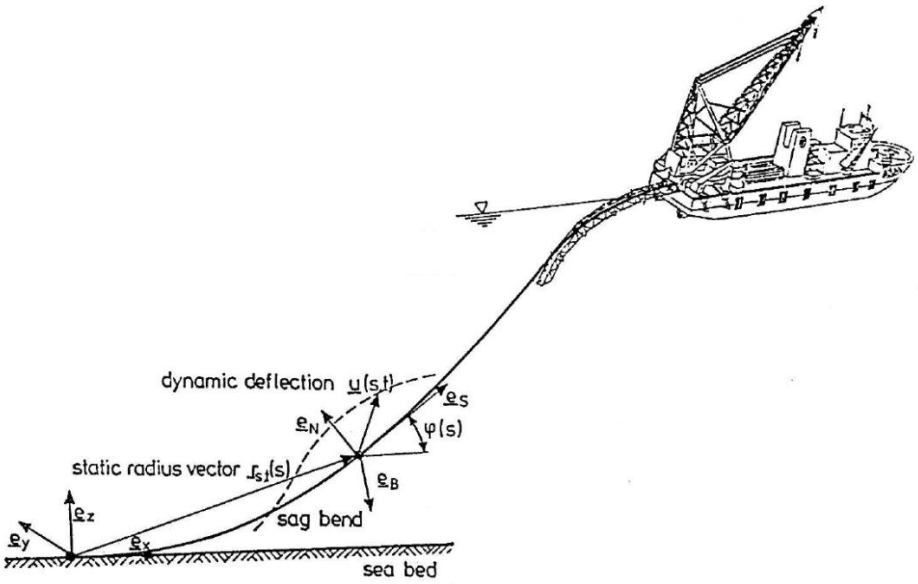

Figure 3: Pipelay problem setup

$u_N(s,t)$ and $u_B(s,t)$ are the lateral deflections of the pipe due to dynamic loads and $\Delta u_S(t)$ is the dynamic motion of the tensioner. $F_{S_{st}}$ and $F_{S_{dy}}$ together comprise the total effective tension force.

Clauss et al. [2] accounts for *hydrodynamic damping* in (23) and (24) as:

$$b = c_d \frac{\rho D}{2}\sqrt{(\dot{u}_N - v_N)^2 + (\dot{u}_B - v_B)^2} \tag{27}$$

These equations are solved iteratively using the Galerkin method to produce a finite-element-type problem using the system matrices for damping [*B*] and stiffness [*C*]. Finally, the

system is solved in the time domain resulting in the *total longitudinal stresses* (bending plus axial) given by:

$$\sigma_S = \frac{F_{S_{st}} + F_{S_{dy}} - \rho g (d_0 - z_{st}) \frac{\pi D^2}{4}}{\pi t_s (D_{se} - t_s)} \pm \frac{1}{2} E D_{se} \sqrt{(\varphi' + u_N'')^2 + u_B''^2} \tag{28}$$

Clauss stated that dynamic amplification of pipe stresses is caused by vessel motions and surface wave loads on the pipe. Although his work only considered vessel motions, he noted that for rigid stinger operations, the wave loads could be neglected and for articulated stingers the effects were roughly 30% of the vessel motion loads. Another interesting result of this research was that the free span pipeline does not affect vessel motions anywhere except near the natural frequencies for heave and pitch due to the additional viscous damping terms in these degrees-of-freedom.

In shallow water S-Lay operations, buckling is not as concerning as longitudinal bending stresses, but should still be considered in the analysis. The critical buckling pressure on a circular pipe is:

$$p_{cr} = \frac{2E}{(1-\nu^2)\left(\frac{D}{t}\right)^3} \tag{29}$$

where ν is the Poisson's ratio, *E* is the modulus of elasticity, and *D/t* is the diameter to wall thickness ratio of the pipe.

For most flows, the *circumferential stresses*, σ_φ, are negligible when compared with the bending stresses, σ_S, but they can be added together through the distortion energy hypothesis as in Clauss et al. [1] to determine the equivalent stress.

$$\sigma_{eq} = \sqrt{{\sigma_S}^2 + {\sigma_\varphi}^2 - \sigma_S \sigma_\varphi} \tag{30}$$

DNV [5] provides an "Offshore Standard" for pipeline installation and planning, DNV-OS-F101. The document was written with the objective of ensuring pipeline systems are safe for

the public and the environment. DNV states that "the operating limit conditions shall be based on stress and strain calculations," and provides the table below for the *Specified Minimum Yield Strength* (SMYS) and *Specified Minimum Tensile Strength* (SMTS) for API grade pipes. This work will consider API X65 grade pipelines.

Table 1: API Material Grades for Pipelines

API Grade	SMYS		SMTS	
	ksi	MPa	ksi	MPa
X42	42	290	60	414
X46	46	317	63	434
X52	52	359	66	455
X56	56	386	71	490
X60	60	414	75	517
X65	65	448	77	531
X70	70	483	82	565
X80	80	552	90	621

DNV [5] also provides criteria for the total allowable stress and strain in a pipe laying analysis, depending on the incorporation of dynamic loading in the model. These strains should include all effects of bending, axial forces, and local roller loads.

Table 2: Allowable overbend strain

Criterion	X70	X65	X60	X52
Static	0.270%	0.250%	0.230%	0.205%
Static & Dynamic	0.325%	0.305%	0.290%	0.260%

The sagbend has a slightly lower allowable limit, written in terms of equivalent stress:

$$\sigma_{eq} < 0.87 \cdot SMYS \tag{31}$$

Equation (31) applies to the combined static and dynamic loads and includes the longitudinal and circumferential stresses. The limit can be rewritten in terms of strain as:

$$\varepsilon < \frac{0.87 * SMYS}{E} \tag{32}$$

It should be noted here that the pipeline is allowed to exceed the yield stress in the overbend region, that is, near the vessel as the pipe exits the stern. The pipe profiles in Figures 1 and 2, shown previously, indicate the significant bending experienced as the pipe becomes unsupported externally.

For example, an X65 grade pipe has a total allowable strain, ε, of 0.305% (Table 2) which is beyond the SMYS of the pipe (448 MPa / 65 ksi) from Table 1.

$$\varepsilon = 0.305\% = \frac{\sigma}{E} = \frac{\sigma}{200{,}000\ MPa} = 610\ MPa\ (88.45\ ksi) \tag{33}$$

Thus, the pipe is yielding when the allowable limit is reached.

2.6. Pipeline Hydrodynamics

For slender tubular members with a characteristic dimension less than $\frac{WL}{5}$, where WL is the wave length, a strip theory approach to computing drag loads can be made. The Morison equation was developed in 1950 to estimate the wave loads on slender cylinder structures such as oil platform support legs. The equation is the sum of the linear inertia force from potential theory and the quadratic drag force from cross-flow on a strip of the cylinder [6].

$$dF_M = F_{intertia} + F_{drag} \tag{34}$$

$$dF_M = \rho C_m \frac{\pi}{4} D^2 \dot{u} + \frac{1}{2} \rho C_d A u|u| \tag{35}$$

The first term in (35) is the inertia force composed from the Froude-Krylov force and the hydrodynamic mass force where C_m is the mass coefficient which depends on the cross-section of the pipe and accounts for added mass.

$$C_m = 1 + C_a \tag{36}$$

For potential flow theory, C_a=1 for a fixed cylinder in waves [12].

The second term in (35) is the drag force where *A* is the projected cylinder area perpendicular to the flow. In the case of the pipeline, this is the water depth, *WD*, multiplied by the cylinder diameter, *D*.

$$F_D = \frac{1}{2}\rho C_d (WD \cdot D) u|u| \tag{37}$$

The flow velocity, *u*, can be found using linear wave theory [12] in which the particle velocity and acceleration as a function of depth and time are:

$$u_{wave}(z,t) = \frac{\omega H}{2}\frac{cosh\left[\frac{2\pi}{WL}(z+WD)\right]}{sinh\left[\frac{2\pi \cdot WD}{WL}\right]} cos(\omega t) \tag{38}$$

$$\dot{u}_{wave}(z,t) = -\frac{\omega^2 H}{2}\frac{cosh\left[\frac{2\pi}{WL}(z+WD)\right]}{sinh\left[\frac{2\pi \cdot WD}{WL}\right]} sin(\omega t) \tag{39}$$

A current force can be applied by superimposing the current flow velocity to the particle velocity due to surface waves.

$$u_{total}(z,t) = u_{waves}(z,t) + u_{current}(z,t) \tag{40}$$

Accumulating marine growth on submerged pipelines will increase the hydrodynamic drag and added mass coefficient due to a larger effective diameter, but is not necessary to consider for pipeline installation where the pipe is newly machined. For pipeline removal from the seafloor, the cross-sectional area $\left(\frac{\pi}{4}D^2\right)$ should be increased to account for the added growth.

Equation (35) produces the inline drag force perpendicular to the cylinder axis, but ignores lifting forces due to vortex shedding. This flow phenomenon is not of major concern in pipelaying applications because of the relative small diameter of a pipeline and low Reynold's number flows existing in pipelay installation [7]. Therefore, the Morison equation is sufficient to analyze the effects of the suspended pipeline during installation.

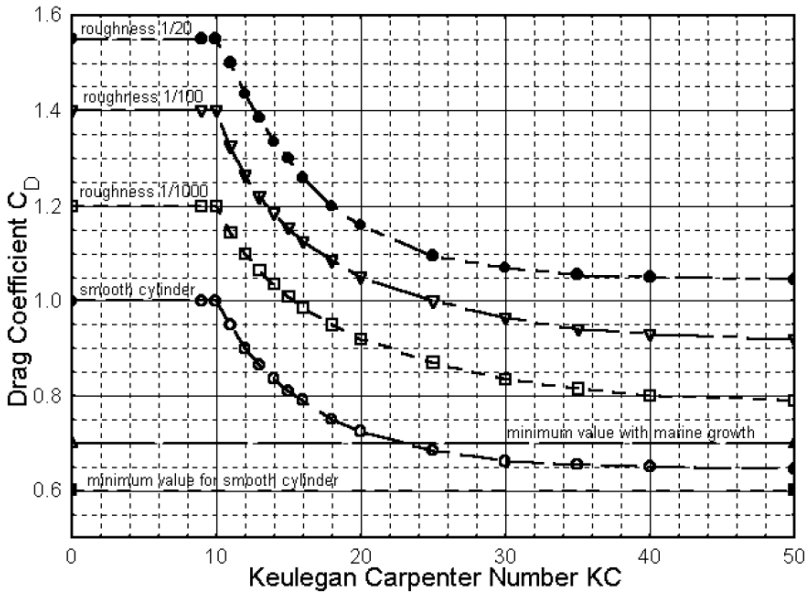

Figure 4: Pipeline drag coefficients (Source: DNV [5])

DNV suggests that the drag coefficient, C_D, be determined from Figure 4 depending on the roughness of the pipe and the Keuligan Carpenter number, *KC.*

$$KC = 2\pi \frac{\zeta_a}{D} \tag{41}$$

MOSES uses the smooth cylinder curve in Figure 4 and allows for manual input of a roughness factor to increase the drag effects from the pipe. The software applies Morison's equation to the discretized pipeline model and computes the associated viscous drag and added mass forces. However, radiation damping is ignored on the pipe element as the slender assumption is made. The drag force is computed for each segment of the pipeline, 100 in all, and then combined into final components acting on the vessel system.

The vessel hull model only has radiation damping applied, but no viscous damping which assumes that the hull is relatively smooth. The stinger model included with the S-Lay configuration contains Morison-type beam elements, and thus, Morison drag is applied to the stinger.

Two methods of solving for the hydrodynamic pressures on the hull area available: two dimensional diffraction theory and three dimensional diffraction theory. While the mathematics of these theories differs, they both compute the excitation force, added mass, and radiation damping for the hull as a function of frequency. For reference, Figure 5 shows the heave and pitch RAO functions as computed using 2-D and 3-D diffraction theory with 900 panels comprising the hull. Due to the sample lay-barge's uniform cross-section, 2-D strip theory performs rather well compared with the more accurate 3-D diffraction/radiation method. Using 2-D theory, the analysis requires less computational time and achieves very accurate results. This work will consider strictly 2-D diffraction theory although it is always recommended to use 3-D diffraction theory when available or where required by detailed geometries.

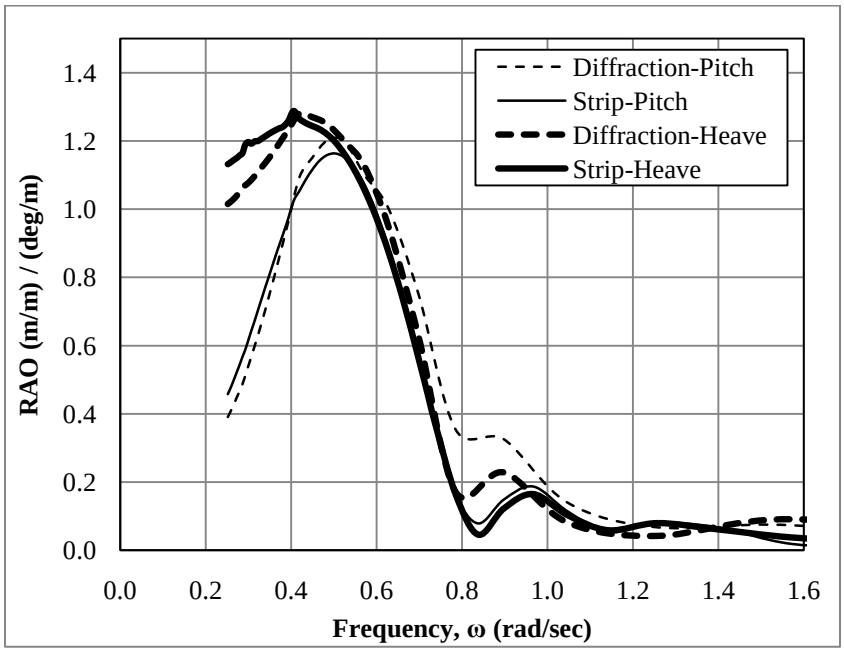

Figure 5: *MOSES* 2-D/3-D Diffraction RAO Comparison

Section 3 - Results

3.1. Wave Energy Density Spectrum Creation

In this section, a random wave signal is considered. The time series motion data is read into a brief subroutine which computes the FFT of the data into the frequency domain as described in (10). The signal is for an actual sea state measured using a North Sea wave probe in light seas with moderate swell conditions.

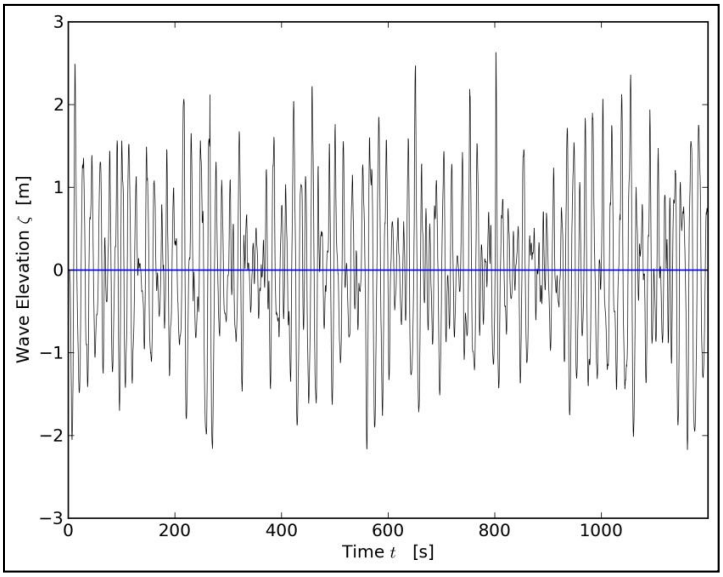

Figure 6: 1200 second time series Hs=1.75m Tm=12 sec (North Sea)

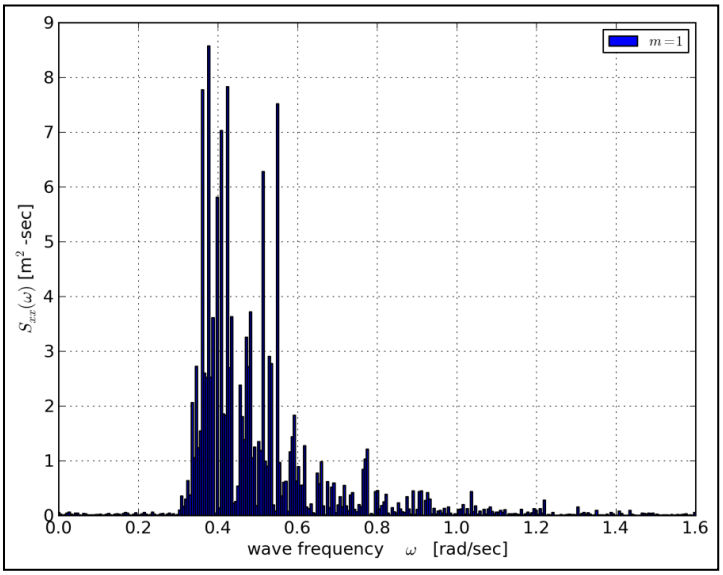

Figure 7: Rough spectra Hs=1.75m Tm=12 sec (North Sea)

As shown in Figure 7, the spectrum is very ragged after the FFT is performed. To maintain better consistency with linear potential theory, it is preferred that the energy density spectrum have a Rayleigh-type distribution. After smoothing the rough spectrum through averaging, the spectrum is shown in Figure 8.

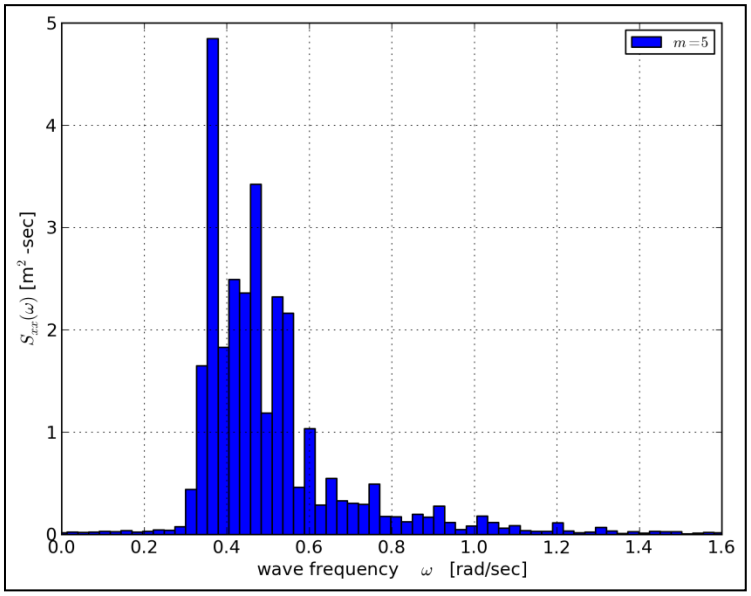

Figure 8: Smoothed spectra Hs=1.75m Tm=12 sec (North Sea)

Five cuts (*m*=5) of the 20 minute (1200 second) time series are sufficient to begin to see the Rayleigh distribution in the above figure. Additional cuts of the time series, to say *m=10*, will begin to lose some of the consistency with the actual sea state. Through integration of the spectrum and its moments, the accuracy of the smoothed spectrum is shown in the table below.

Table 3: Spectrum smoothing analysis (North Sea)

Increment (sec)	**m_0 (m^2)**	**m_1 (m^2/sec)**	**H_s (m)**	**T_m (sec)**
Unsmooth	0.7694	0.3975	1.754	12.162
Smooth *m=5*	0.7692	0.3985	1.754	12.128
0.004	0.7673	0.3985	1.752	12.099
0.02	0.7610	0.3927	1.745	12.175
0.5	0.7459	0.3780	1.727	12.398
1.0	0.7278	0.3720	1.706	12.291

It is still not practical to use all 250 frequency "bins" in the smoothed spectrum, so time/frequency increments are used to limit the amount of data for processing. This, of course, reduces some of the accuracy of the real-time wave data signal, but still maintains less than a 1% deviation and helps with computational efficiency. A 1.0 sec increment between bins seems to be sufficient and more closely follows a Rayleigh distribution for this surface elevation time series. A plot of all of the spectrum approximations is shown below in Figure 9.

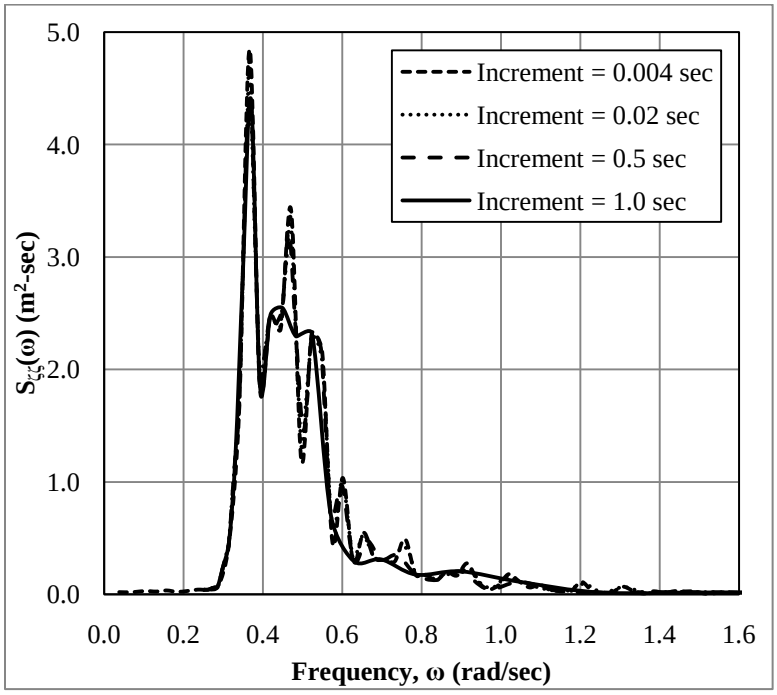

Figure 9: Comparison of frequency bin width on spectrum shape

Data from numerous wave buoys throughout the World's oceans are available for research purposes. The National Oceanic and Atmospheric Administration's (NOAA) National Buoy Data Center (NDBC) database provides access to many of these buoys. Energy density spectra from two specific locations, the Gulf of Mexico and Middle Atlantic are shown in Figures 10 and 11. The NDBC applies an FFT to the vertical displacement measurement obtained by the buoy. Then, RAO processing is performed on the transformed data to account for noise in the signal. It is from this transformation that non-directional spectral wave measurements are derived.

The NDBC publishes the energy density spectrum every hour online, rather than the time series of surface elevation. Three different spectra over three hours from the same buoy are shown below from the Bay of Campeche in the Gulf of Mexico and the Middle Atlantic as well as their average.

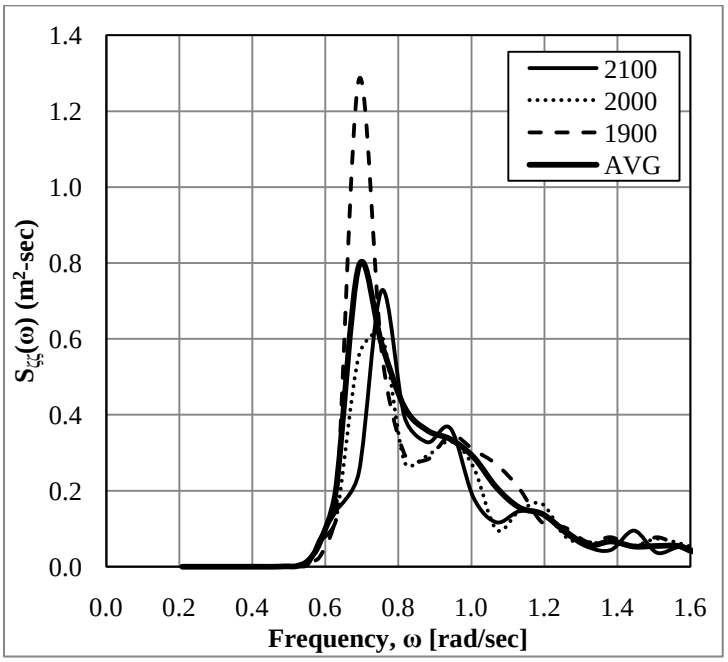

Figure 10: Energy Density Spectra, Buoy #NDBC-42055 Gulf of Mexico

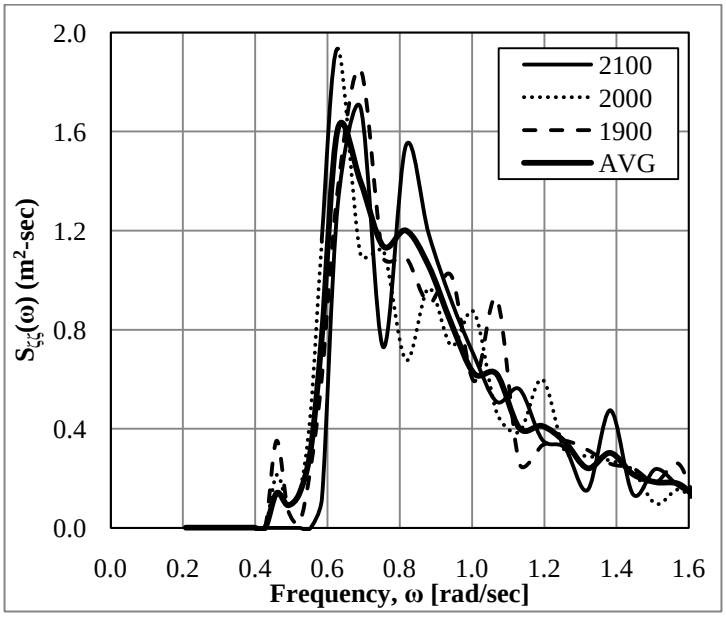

Figure 11: Energy Density Spectra, Buoy #NDBC-41041 Middle Atlantic

As pipelay operations are considered by DNV to be weather restricted (taking place within 72 hours of the last forecast), recent weather data can be used to predict operating quantities, such as motion or stress. As plotted in the figures above, an average spectrum can be estimated by taking the mean of all spectra of interest at each frequency.

$$S_{\zeta\zeta,AVG}(\omega) = \frac{1}{N}\sum_{i=1}^{N} S_{\zeta\zeta,i}(\omega) \tag{42}$$

Here, spectra from the six preceding hours are averaged together to be applied to the vessel system. As can be seen below, at the time of interest, the sea in the Middle Atlantic (NDBC#41041) has considerably more energy than in the Bay of Campeche, Gulf of Mexico (NDBC#42055).

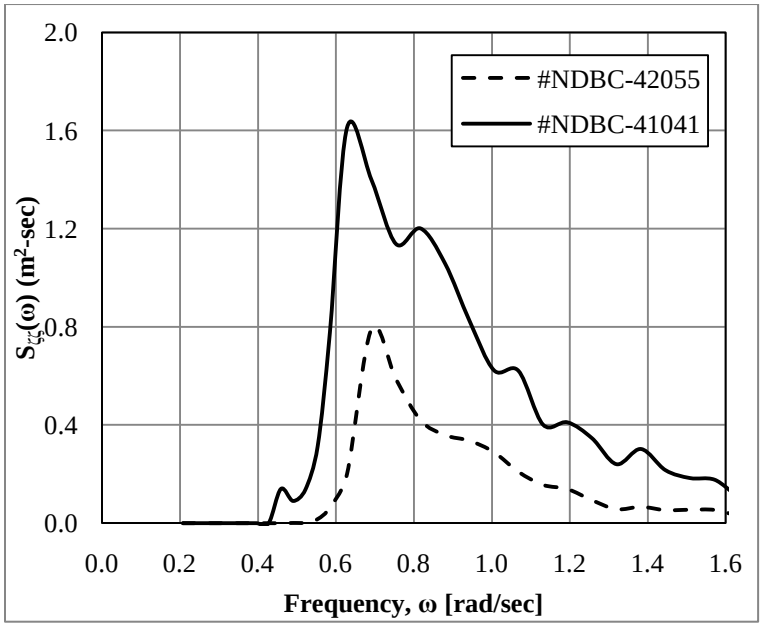

Figure 12: Averaged Energy Density Spectra (6 Hours)

Table 4: Environment Comparison of NDBC Buoys

	NDBC-42055		NDBC-41041	
Time [UTC]	**Hs [m]**	**Tm [sec]**	**Hs [m]**	**Tm [sec]**
1900	2.12	6.65	3.52	6.52
2000	1.89	6.29	3.45	6.62
2100	1.87	6.21	3.43	6.34
AVG	2.04	6.56	3.49	6.55

For future project planning, buoy data can be obtained commercially or a method similar to this can be made if a research buoy in relative proximity to the project site is available. Of course, more than six hours should be considered for installation *planning*. Here, only near-future events are estimated for operational decision-making. Also commercially available are wave scatter diagrams for regions of interest covering decades. The larger sample size helps to remove any unwanted effects from regional storms, currents, tides, etc.

3.2. System RAOs

The RAOs as described in (5) are computed using the hydrodynamic software suite, *MOSES*. Figure 13 presents the transfer functions of interest for pipelay operations in which the seas are coming from the bow, a 180 degree heading. This is typically the worst case for pipelay operations as the waves push the vessel aft causing the pipeline profile to compress, increasing the stresses in both the overbend and sagbend. For project planning, multiple headings must be considered with an even reoccurring frequency distribution as the pipelay vessel operator can rarely position the vessel optimally due to a strict pipeline route.

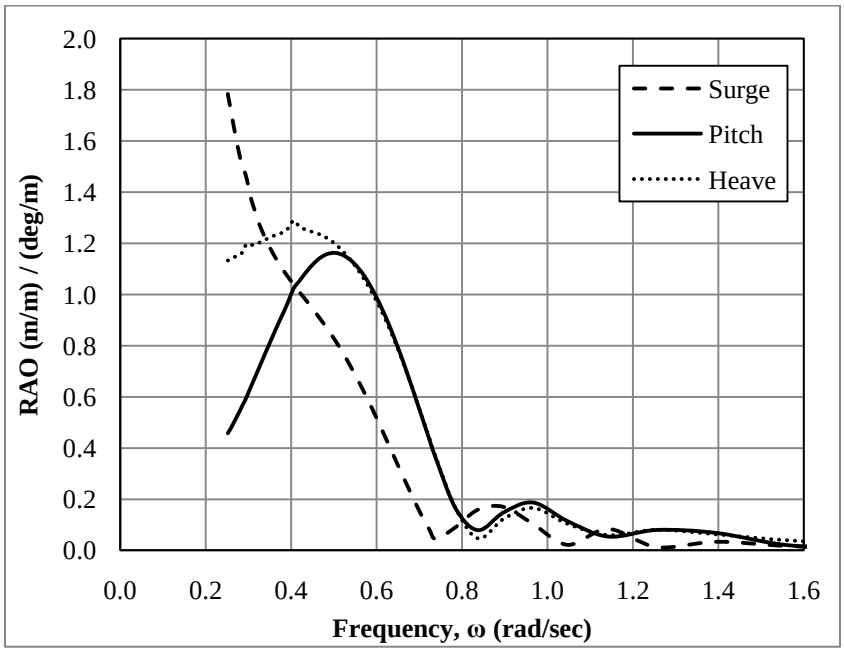

Figure 13: Vessel RAO curves at Pipe Exit, Heading = 180 deg (Head Seas)

A plot of the beam sea (90 deg heading) RAOs are presented in Figure 14 to show the un-damped roll properties of the vessel. In reality, viscous damping is applied to the ship which decreases the peak of the roll RAO curve, but this has not been done here. In most pipelay vessels, roll is not a governing criterion as the pipe exit is located on centerline and subsequently, the vessel simply rolls about the pipe axis. For applications with an off-center pipe exit, roll should be considered, specifically the vertical excursion of the pipe. J-Lay operations also require the consideration of roll on the overbend stresses if the tower is exceedingly tall. However, the static overbend stresses are small or non-existent in this segment of the pipeline and can often be ignored for bending.

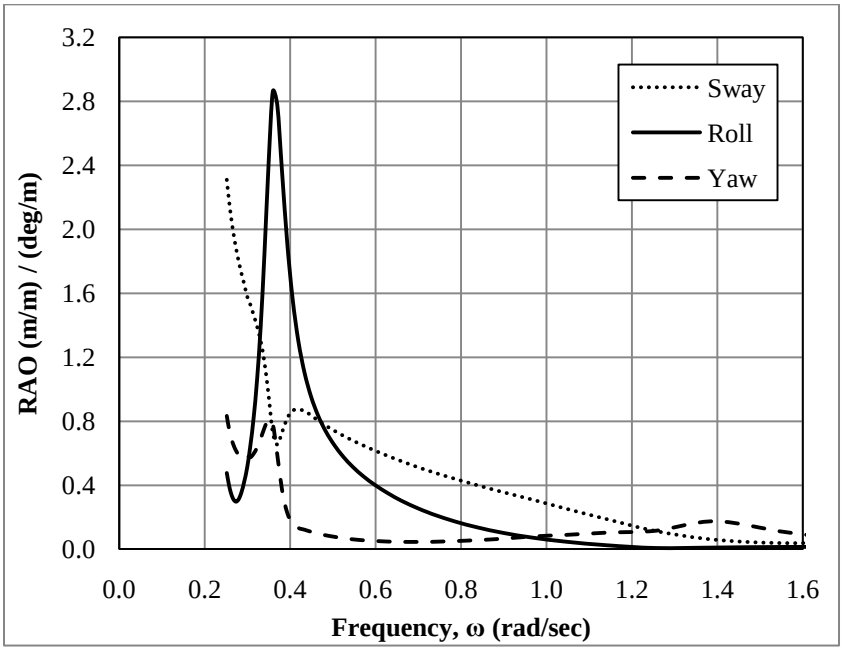

Figure 14: Vessel RAO curves at Pipe Exit, Heading = 90 deg (Beam)

MOSES contains a package for modeling and analyzing the dynamic amplification of stresses in a pipeline by solving the pipeline system for a given top tension, roller locations, and pipe properties. A sample pipeline has been incorporated for computation of the RAOs above. As stated in Clauss et al. [2], the free span pipeline extending from the vessel to the sea bed does not affect vessel motions anywhere except near the natural frequencies for heave and pitch, $\omega = 0.5$

rad/sec, due to the additional viscous damping terms in these degrees-of-freedom. However, its inclusion in the system model helps to more adequately capture hydrodynamic effects including Morison damping forces.

3.3. Pipeline Models

Two pipeline configurations were modeled for both *J-Lay* and *S-Lay*. Both models contain twelve catenary mooring lines and a 16 inch outer-diameter pipeline to capture damping and tension effects. In the *J-Lay* configuration, shown below, the pipe slopes down a tower at about 50 degrees above deck, held at the top by a tensioner, and restricted by two clamps in the tower. This case is shallow water for J-lay operations, but offers a good comparison of pipeline profiles to S-Lay shown following.

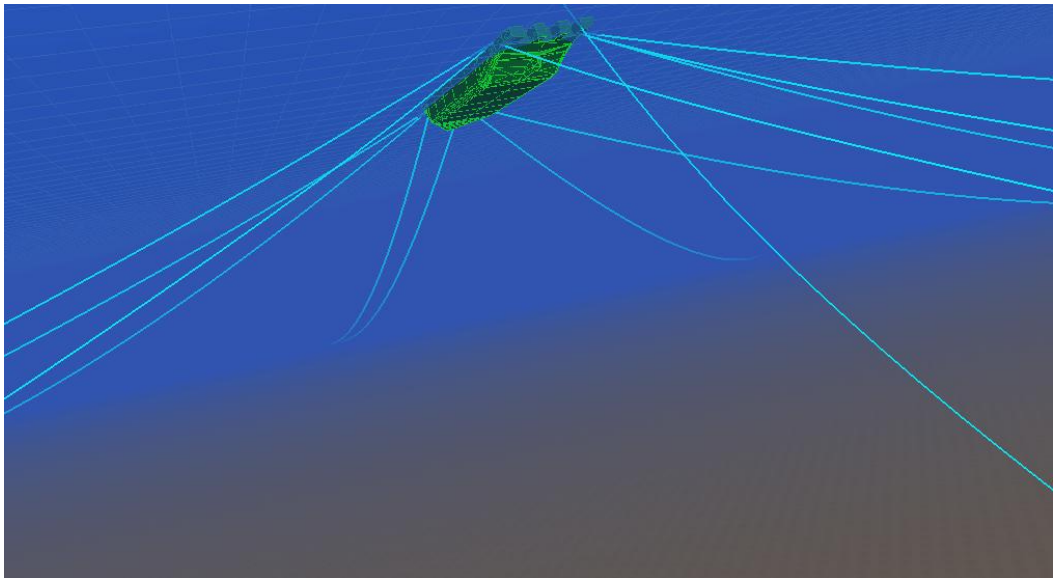

Figure 15: Typical Lay Barge Pipelay Model in *MOSES* (J-Lay)

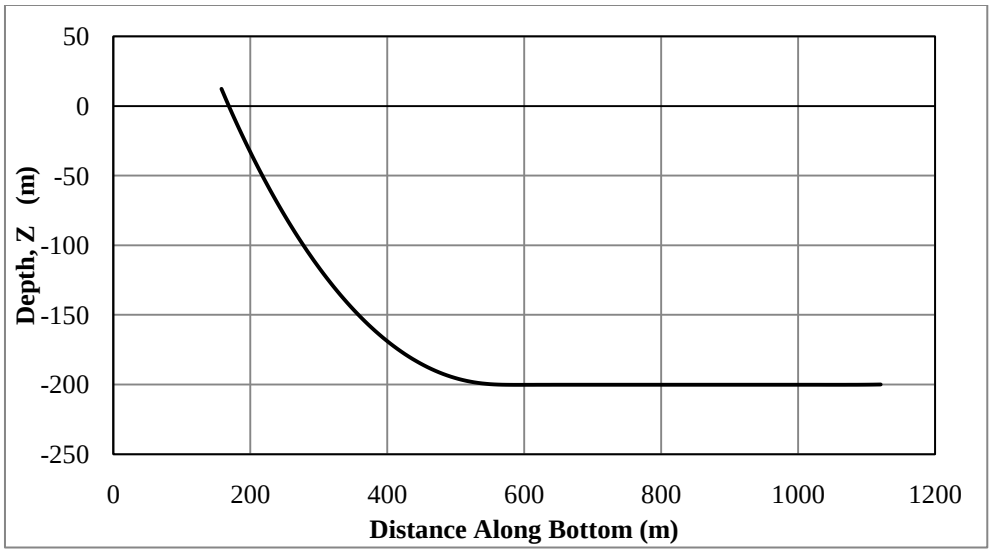

Figure 16: Pipe profile in 200 m water depth (J-Lay)

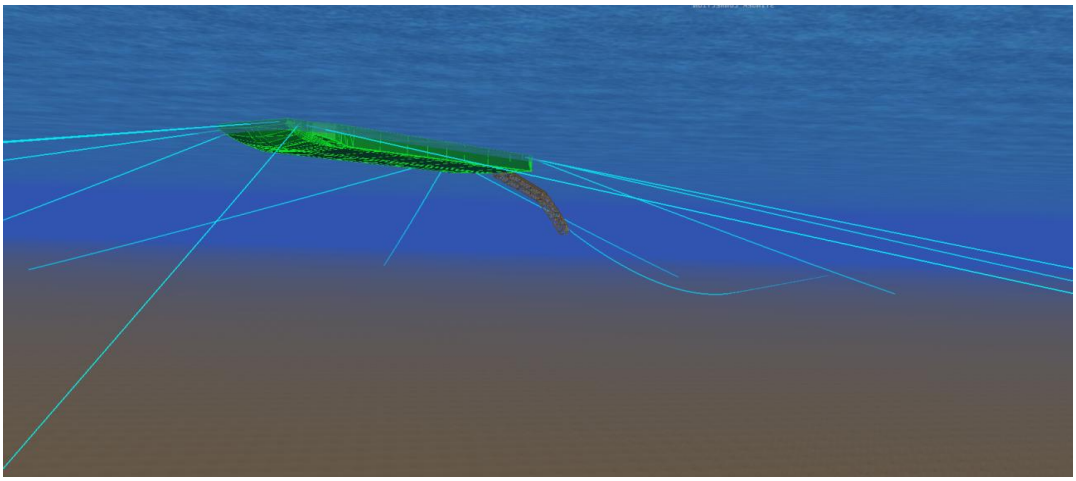

Figure 17: Typical Lay Barge Pipelay Model in *MOSES* (S-Lay)

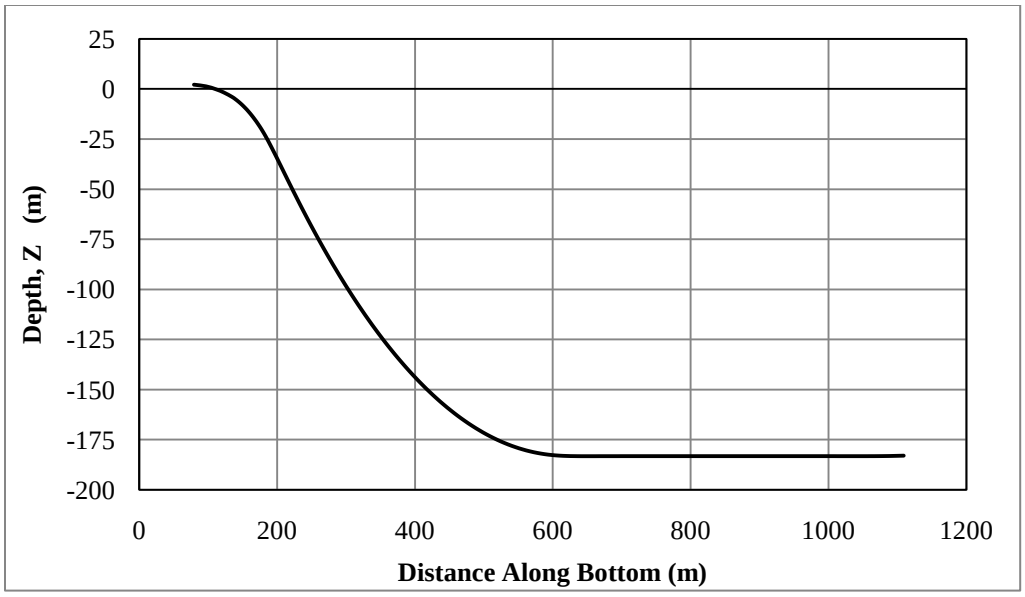

Figure 18: Pipe profile in 182 m water depth (S-Lay)

In the *S-Lay* configuration, the pipe slopes down a centerline pipe ramp and exits onto a stinger containing a series of roller constraints allowing only vertical movement (i.e. liftoff). The tip of the stinger is called the "lift-off point" (LOP) and is often the location of the highest bending stresses as the pipe begins its free-span to the sea floor. Adjusting the stinger radius shorter (angled-down), the LOP will take less load, but the pipe will also experience more bending stresses in the sagbend. Pipeline installation is a sensitive operation and numerous cases of the applicable variables are tested for the specific scenario at hand. For example, larger pipelines react differently than smaller pipes and cannot handle as small a bending radius. Detailed pipeline mechanics and installation procedures will not be addressed here in this vessel dynamics study. There is, however, much technical material available on this subject [7, 8].

Here, the S-Lay model is considered for the purpose of explaining the method, but the setup can easily be used on a J-Lay system as well. A plot of the static longitudinal stress distribution is shown below. The inflection point, or cross-over between the overbend and sagbend exists near 210 meters from the bow reference point (0 meters along bottom) where the

bending stresses go to zero and only small axial stress in the pipe remains. After lay down of the pipe at about 600 meters along the bottom, the bending stresses diminish rapidly, leaving only axial stress due to the applied tension force.

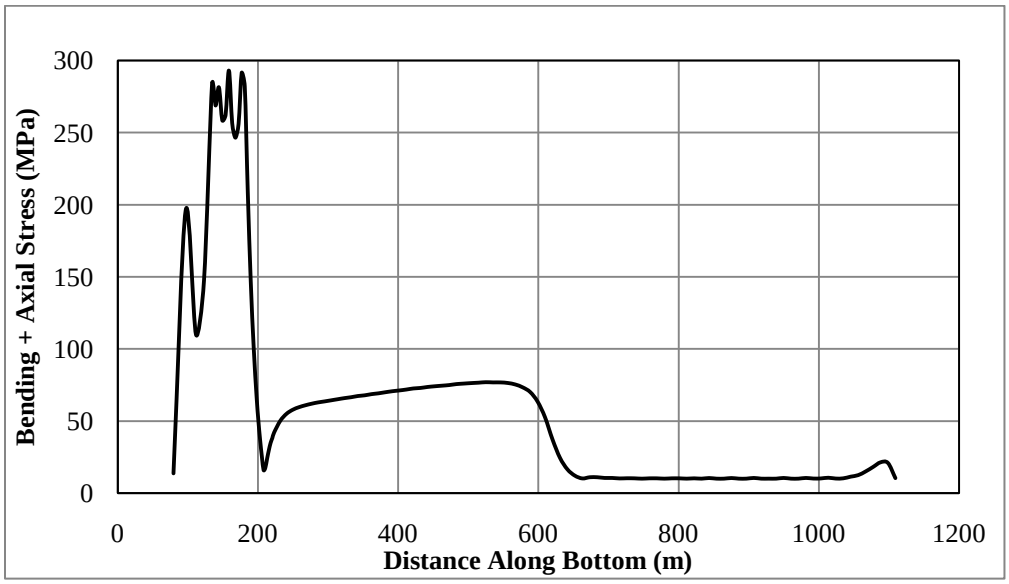

Figure 19: Static longitudinal stress in pipeline (S-Lay)

Figure 19 depicts the large bending stresses located on the pipe support rollers on the vessel and stinger. The pipe model begins near 80 meters from the bow with relatively low longitudinal stress. Then, as the pipe spans the rollers, bending stresses increase until exiting the stinger at about 200 meters from the bow.

For a brief comparison, a plot of the static longitudinal stresses in a J-Lay configuration is shown below. The stresses in this J-Lay example are on the order of half in S-Lay due to the absence of large local support reactions from rollers or a stinger. The J-Lay pipeline is supported by a single point, the tensioner, eliminating much of the local spike reactions shown in Figure 19. As the water depth increases, sag bend stresses will begin to quickly rise which ultimately limits the capability of a lay vessel. Refinement of the roller heights, vessel trim, and stinger radius can lower the high stresses at these locations, but this model is sufficient to progress.

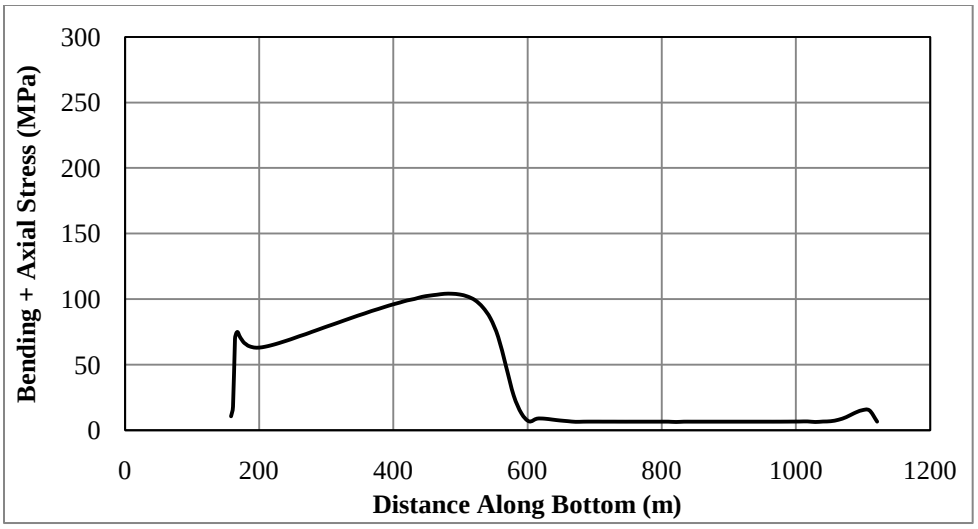

Figure 20: Static longitudinal stress in pipeline (J-Lay)

3.4. Dynamic Pipeline Stress

The dynamic longitudinal stress component is linear from the assumptions made earlier with vessel dynamics. Figure 21 shows this assumption to be valid in the model with three significant wave heights with identical periods, directed from the bow. The stresses increase linearly with wave height along the entire pipe length. The dynamic axial stresses are approximately 30% of the total normal stress in the sag bend compared to only about 15% in the static case. Hence, axial stresses should carry extra consideration when pipelaying in marginal environments.

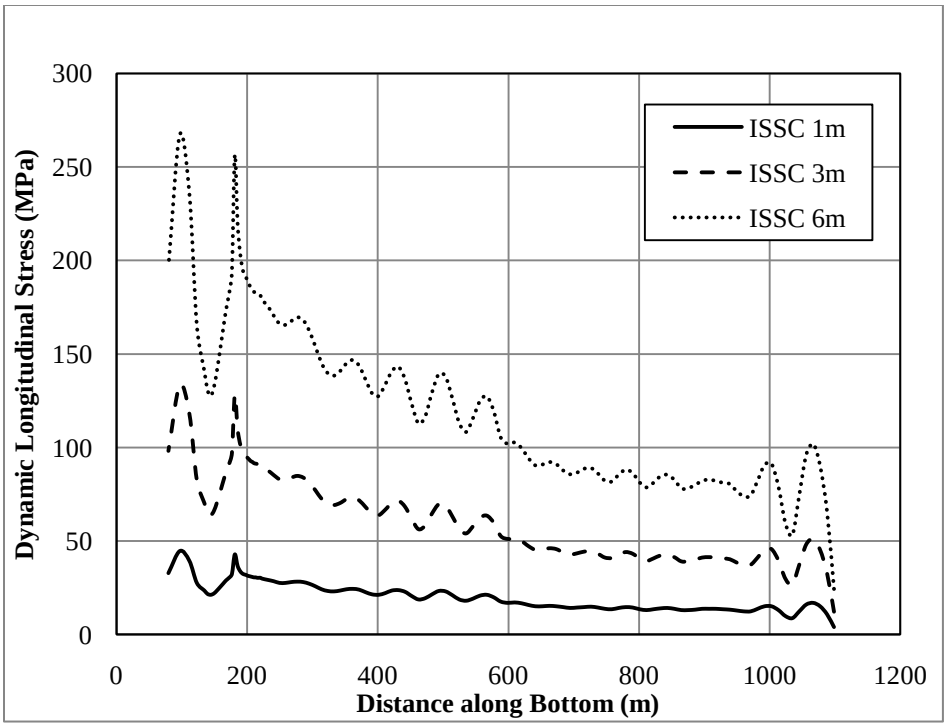

Figure 21: Dynamic longitudinal stress in pipeline, Tm = 5 seconds

The ISSC irregular wave spectrum is used to demonstrate the linear properties of the pipeline stress analysis in the figure above, although this holds true for any spectrum. The stress curve for a 3 meter significant wave height is simply three times the one meter curve. To show the influence of the wave period, the dynamic stress is plotted for an ISSC spectrum with a one meter significant wave height and various mean periods (Figure 22). The upper most curve (blue) represents a mean period of 3 seconds, while the lowest curve (gray) shows the highest period checked, 25 seconds.

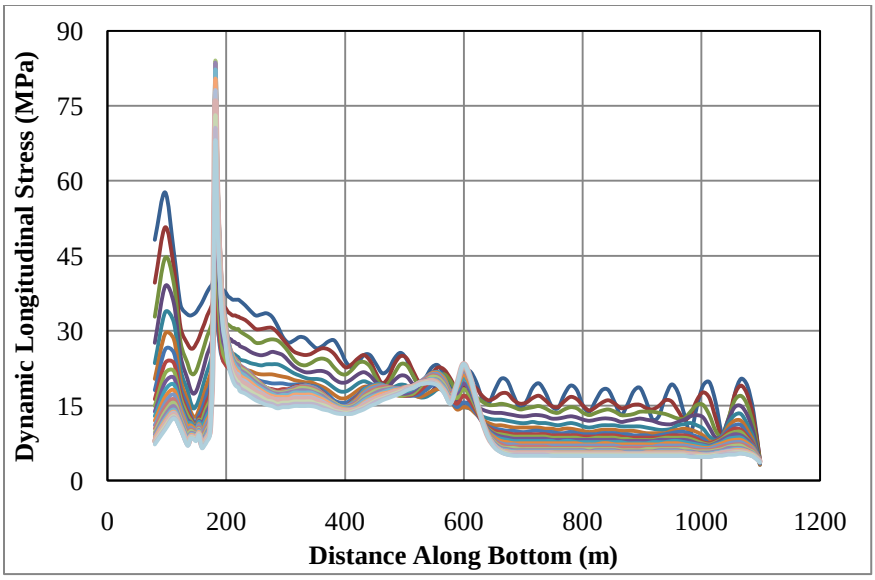

Figure 22: Dynamic longitudinal stresses, ISSC Hs=1m, Tm=3-25 sec

The total longitudinal stress is found by superimposing the static and dynamic components.

$$\sigma_{TOTAL}(\omega) = \sigma_{STATIC} + \sigma_{DYNAMIC}(\omega) \tag{43}$$

It is often important to know how the system will respond in a particular environment such as a field check by a vessel superintendent to determine if the vessel can begin or continue to work, or by a project planning team to predict the ship's effectiveness in carrying out a specific operation.

3.5. Limiting Sea State

Offshore construction companies typically develop limiting sea state curves for specific vessel operations, such as heavy crane lifting, ROV lowering, or pipelaying. In most cases, only the hull is considered in the hydrodynamic model, although mooring lines and a stinger are also included in some instances. Specific software (e.g. *Orcaflex*) has been developed in the last three decades to assist pipeline engineers with determining the limiting sea states for pipelaying operations. Ship RAOs can be input from a hydrodynamic suite (e.g. *MOSES* or *WAMIT*) and the pipeline can be analyzed for the total stresses, both static and dynamic in specific environments.

In this work, the static stress curve presented in Figure 19 is combined with the dynamic stresses shown in Figure 22 to determine the limiting sea state using the linear assumption and superimposition. The allowable significant wave height for each period is determined by satisfying:

$$\sigma_{STATIC} + H_S \cdot \sigma_{ISSC,\,1/50{,}000} \leq \sigma_{ALLOWABLE} \tag{44}$$

where $\sigma_{ALLOWABLE}$ is conditional on the location along the pipe. The allowable stress is higher in the overbend (Table 2) than in the sagbend as the pipe reaches the seafloor (33). The dynamic stresses can be computed as an RAO (unidirectional regular waves with unit amplitude and single frequency) or using an irregular wave spectrum with a unit amplitude. The latter is considered more appropriate than regular wave analysis to find limiting sea states since moderate wave heights with random wave properties and directions are more likely to be encountered during pipeline installation.

Figure 23 presents the limiting sea state, H_S, across the frequency range at which the longitudinal pipeline stress (bending plus axial) reaches the value allowed by DNV in the overbend or sagbend. The dynamic stresses are computed with an ISSC spectrum and a statistical multiplier of 1/50,000 as in equation (17). This represents that the pipeline stress should not be exceeded in 72 hours in a sustained environment. As a note of caution, in reality the environment is entirely stochastic and impossible to fully determine. Thus, it is possible for statistically improbable waves to arise in a specific environment resulting in exceeded pipe stresses. However, statistical theory maintains this should not happen and provides a reasonable basis from which to make decisions. Certain precautions should always be taken when operating in a marginal environment and factors of safety applied where desired.

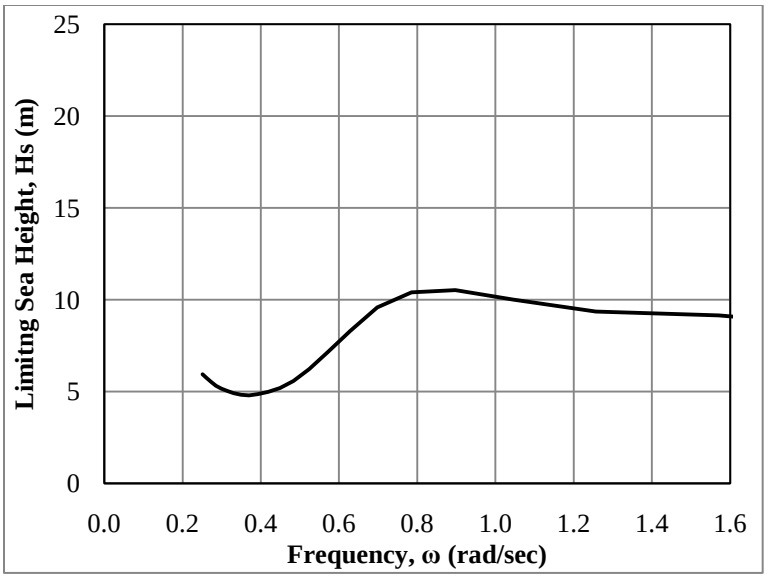

Figure 23: Limiting sea state for pipeline stress (Head seas)

Figure 23 is better considered when paired with the traditional limiting sea state curve for pipelaying, that which governs pitch motion. The pipeline profile is highly dependent on vessel pitch angle and excessive deflection can cause bending or buckling failure in the pipeline. Operations are often governed by the maximum, 1/1,000th pitch angle of 1.5 degrees, single amplitude. Of course, other statistical variations of this limit exist, but the concept is the same. The vessel shall not rotate beyond some maximum value which limits equipment and/or crew operability.

The limiting sea curve for vessel pitch is generated, again, using a unidirectional ITTC irregular wave spectrum across the frequency range.

$$H_S \cdot Pitch_{ISSC,H_S=1m} \leq 1.5 \deg Pitch_{1/1,000} \tag{45}$$

$$H_S \leq \frac{1.5 \deg Pitch_{1/1,000}}{Pitch_{ISSC,H_S=1m}} \tag{46}$$

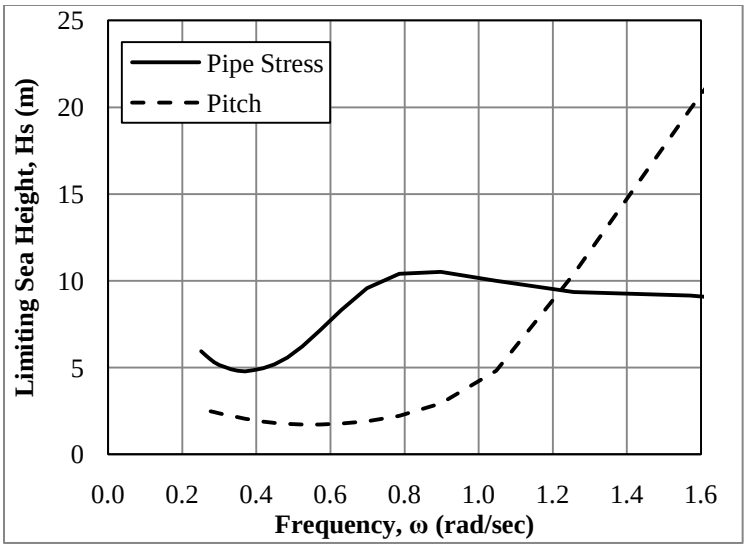

Figure 24: Limiting sea state curves for pipelay operations (Head seas)

The lowest value of the two curves at each frequency is used to determine the composite limiting sea state using both the traditional vessel pitch criterion as well as the effective pipeline stress limit developed here.

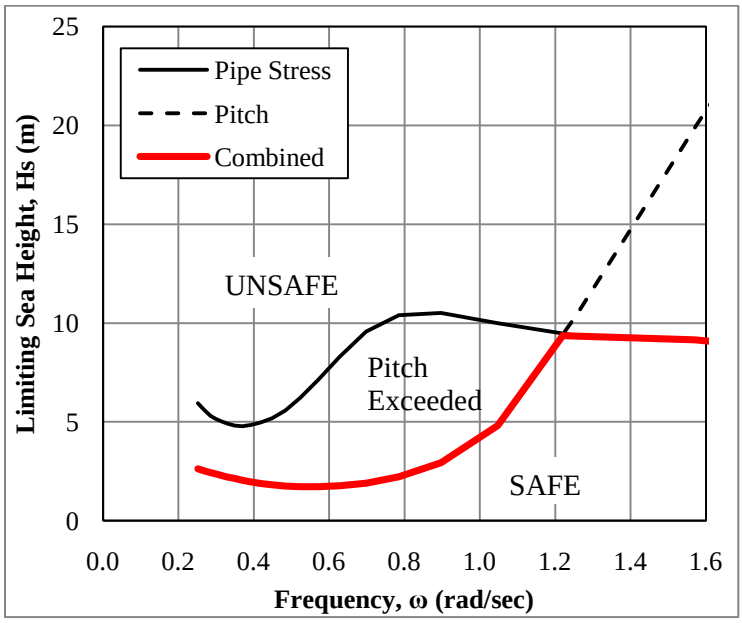

Figure 25: Composite limiting sea state curve (Head seas)

From the figure above, the pipeline stress criterion actually provides a lower allowable sea state for short period, high frequency environments ($\omega > 1.2$ rad/sec) than the traditional

vessel pitch criteria. However, the limiting sea state values in this frequency range are unrealistic (9 meters, 6 second mean period). In the longer period, low frequency environments, (ω = 0.3-1.2 rad/sec) the traditional pitch limit seems to be overly conservative in limiting operations. The pipeline stresses actually permit a much higher allowable sea state. This is not to say that the pitch limit should be fully neglected as the pipe stress limit would actually permit up to a 7.0 degree single amplitude pitch angle (14 degree double-amplitude) before allowable stresses were exceeded. Certainly, no offshore construction company would permit this, considering today's safety standards. In reality, there are additional factors which limit operations including equipment and foundation design restraints and human factors such as human performance. These factors may limit operations prior to the pipeline stress being exceeded, but it is not unreasonable to suggest that the traditional curves may be overly restrictive for project planning and operability index forecasting or "*workability*."

3.6. Workability

In planning any offshore project, it is necessary to predict the required length of time to complete the work. Workability analysis provides a good tool for estimating project duration as well as comparing two vessels with the same task. Downtime percentages are often used in lump-sum project bids to estimate the vessel day-rate and project cost.

Composite limiting sea state curves for each heading of interest are used together with weather statistics shown in a wave scatter diagram at the specific offshore site of the proposed work. To estimate the total percentage of time the vessel is able to work at each heading, the wave percentages of occurrence are cumulatively added until the limiting sea state value is reached. For example, if the percentage of occurrence of the sea state with H_S = 0.5-1.0 meters and T_M = 4-5 seconds is 15% and this window is below the limiting sea curve, the vessel can work 15% of the time. Adding all of the percent of occurrence "boxes" and comparing them with

the limiting sea curve provides the overall workability for that heading. This is repeated for each heading as the limiting sea curves change with vessel orientation. The workability is usually referenced as a percentage, although the number of down days can also be reported per month or year.

$$Down\ Days = (1 - Workable\ \%) \cdot \#\ Days\ in\ Month/Year \tag{47}$$

This can be shown monthly, seasonally, or yearly depending on the information desired [11].

3.7. Real-time Analysis

Earlier, a method was presented for analyzing a time series of wave elevation and converting the data into an energy density spectrum which could then be smoothed (Figure 8). From the statistical properties of the time series, the significant wave height (16) and mean wave period (18) can be determined and plotted against the limiting sea curves as shown below.

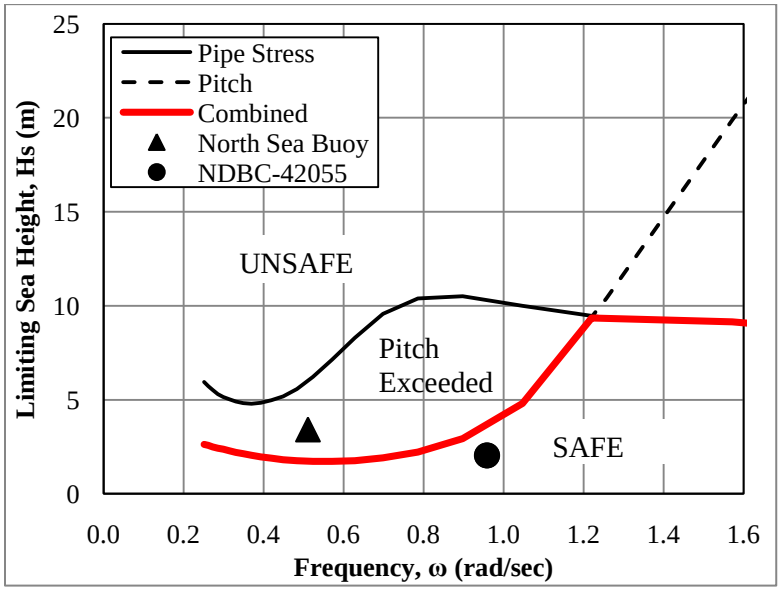

Figure 26: Evaluation of sea state against limiting sea curves

Comparing the actual sea state properties to the limiting curve allows the operator to quickly determine the safety of the vessel in the current environment. This method is typical throughout the offshore construction industry and is general maritime practice for vessel loading assessment.

Here, a more accurate method for predicting the response in the current environment is shown. This methodology was proposed by Legras and Wang [9] in accordance with DNV [4] for subsea crane operations, but is extended here for pipelaying. Using vessel MRU data directly and computing the pipe stresses is preferred over beginning with wave data and estimating the vessel response and pipe stresses, as one can be assured that all hydrodynamic properties of the vessel are properly captured. These include added mass, damping, line tensions, wind, and current. However, time series data is not always available, especially for pipeline stresses so this method will be presented beginning with wave data.

Time series wave data can be applied to the model in the time domain if specific software (e.g. *Orcaflex*) is available. Solving the six-degree of freedom equation of motion is not simple, although it can be done using a finite-difference algorithm. Working in the frequency domain is more computationally efficient and is rather effective for linear systems. Here, the elevation time series is converted to the frequency domain through an FFT as previously described in (10).

From the smoothed wave spectrum, the response spectrum is estimated by squaring the RAOs multiplied to the environment spectrum as in (22). The vessel pitch response is:

$$S_{55}(\omega) = S_{\zeta}(\omega) \cdot RAO_5(\omega)^2 \tag{48}$$

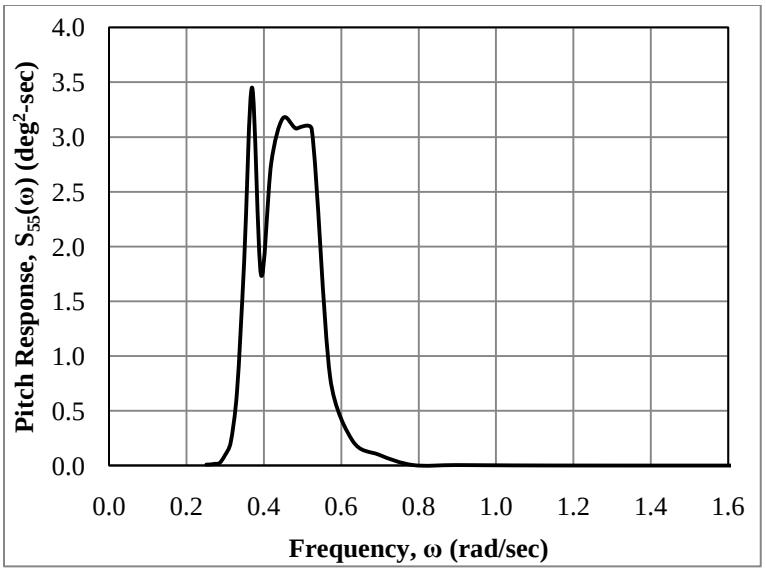

Figure 27: Pitch response spectrum (North Sea)

It is evident in the figure above that there is a sharp drop of "pitch-energy" around ω = 0.4 rad/sec resulting from a similar property of the energy density spectrum (Figure 8). This un-Rayleigh-type distribution loses some of the statistical accuracy of the method which can result in skewed results. Progressing carefully, from the response spectrum in (48), statistical properties like the 1/1,000th value can be obtained.

$$\theta_{5,1/1000} = 3.72\sqrt{\int S_{55}(\omega)d\omega} \tag{49}$$

The transfer function for the pipeline stress requires a bit more attention. The total stress is composed of both static and dynamic components, unlike motion which is purely dynamic. Therefore, the RAO of stress should consider only the dynamic component as a function of frequency, and the static component superimposed after the dynamic stress is computed.

RAOs for both the sagbend and overbend should be derived separately as the allowable stress in each region is different. Only the maximum value of stress on either side of the curvature inflection point is needed for each frequency, although it is possible to generate a dynamic stress RAO for any specific node of interest. A plot of the longitudinal stress RAOs is shown in Figure 28.

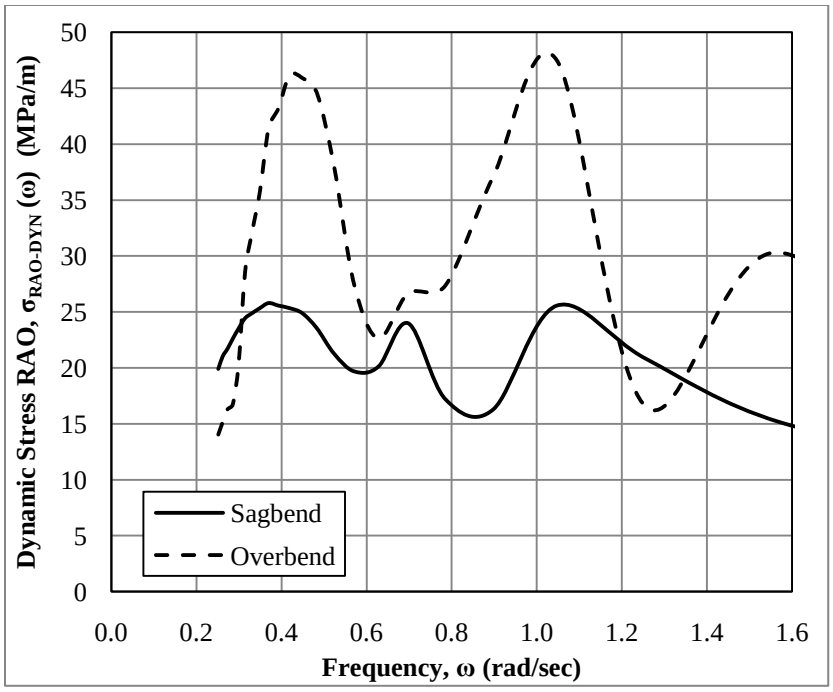

Figure 28: Dynamic stress RAOs (Head seas)

The RAO curves have an oscillatory shape due to the usage of the maximum stress value along the length of the pipe, rather than focusing on a single node. The overbend stresses are larger than the sagbend stresses in this case. Certainly, changing various parameters, such as pipe weight, tension, and the pipe supports will greatly change these curves. Typically, optimizing the static stresses is sufficient for developing an installation procedure although pipeline engineers may consider the dynamic stresses if warranted in a proposed environment or with large pipe sizes.

After computing the dynamic stress RAO curves, the stress response spectrum, $S_{\sigma_{DYN}}(\omega)$, is generated similar to the pitch response spectrum.

$$S_{\sigma_{DYN}}(\omega) = S_{\zeta}(\omega) \cdot \sigma_{RAO-DYN}(\omega)^2 \tag{50}$$

where $\sigma_{RAO-DYN}(\omega)$ is the dynamic stress RAO computed using regular waves with unit amplitude, ζ_a=1 meter, at various frequencies.

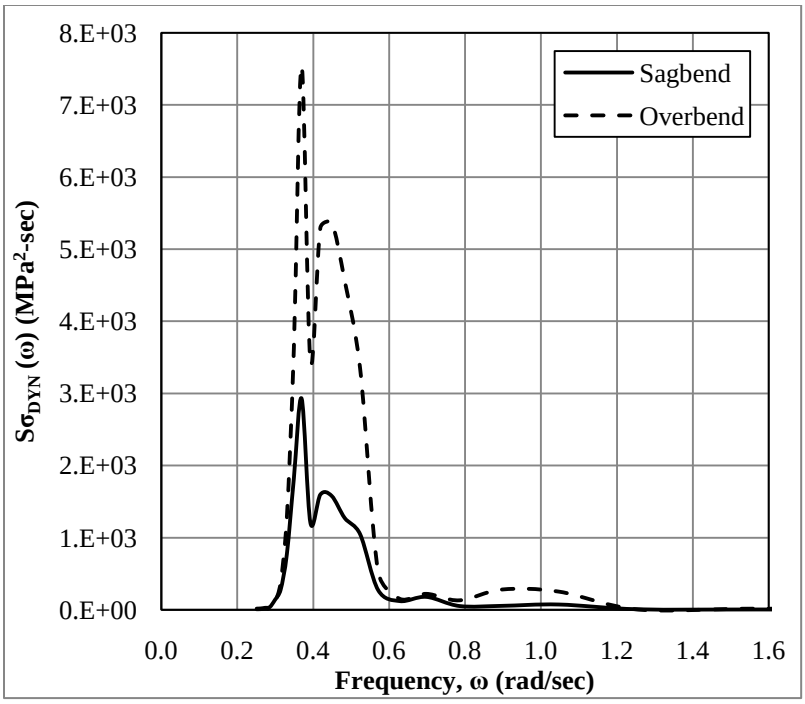

Figure 29: Dynamic stress response spectrum (North Sea)

Again, statistics can be used to determine the largest total stress expected in about 72 hours, or 50,000 waves.

$$\sigma_{1/50,000} = 4.652\sqrt{\int S_{\sigma_{DYN}}(\omega)d\omega} + \sigma_{STATIC} \tag{51}$$

Table 5: Statistical response properties and assessment (North Sea)

Pitch (1/1000)	3.04	deg
Allowable (1/1000)	1.50	deg
	103%	**Fail**
Sagbend Stress (1/50,000)	171	MPa
Sagbend Allowable (1/50,000)	390	MPa
Sagbend	**-56%**	**Ok**
Overbend Stress (1/50,000)	451	MPa
Overbend Allowable (1/50,000)	610	MPa
Overbend	**-26%**	**Ok**

Using the real-time data, the vessel pitch angle more than doubles the allowable value set forth in the traditional pipelay limit (103% exceedance). However, the total sagbend and overbend stresses, considering both static and dynamic effects, are each below the DNV allowable values in this sea-state. Figure 26 shows that this environment should produce pitch motion exceeding the allowable value by about double the limit, but still well within the pipe stress limiting sea state. The statistics in Table 5 above confirm that this is the case.

The process is briefly shown again for the NDBC buoy in the Gulf of Mexico which contains averaged data over six hours, the minimum length of time recommended for making real-time predictions using statistics. The energy density spectrum is shown in the figure below and represents a sea state with significant wave height, H_s, of 2.04 meters and a mean period, T_M, of 6.56 seconds (ω=0.95 rad/sec).

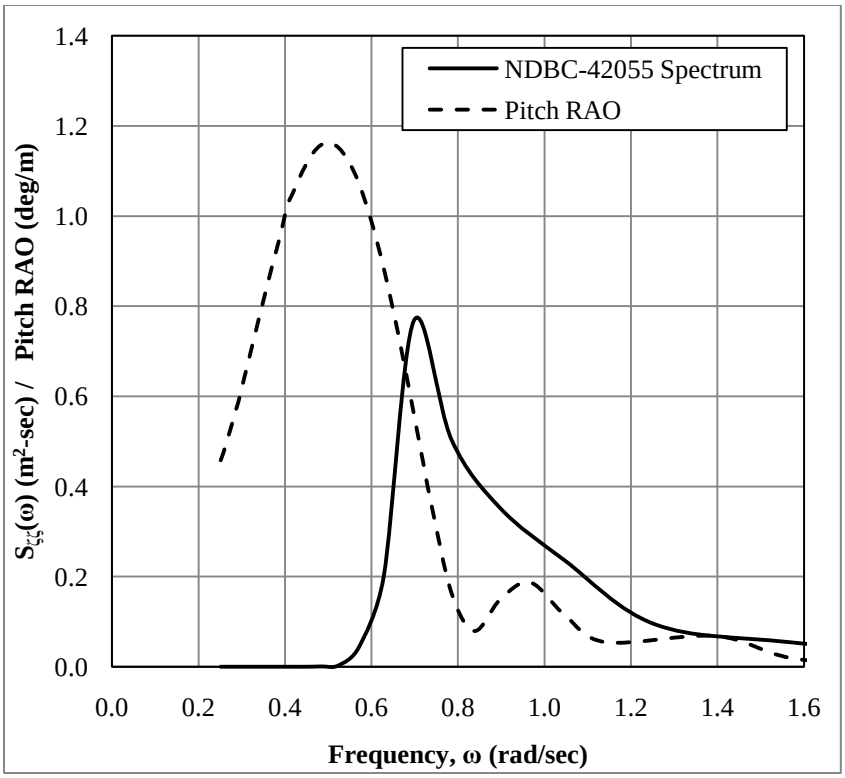

Figure 30: Energy density spectrum (Buoy #NDBC-42055) and Pitch RAO

The energy density spectrum shows a much greater similarity to a Rayleigh distribution indicating a good time sample from which to make statistical decisions. In Figure 30, the vessel pitch RAO is overlaid on the frequency range to note that the peak period of the sea state and the pitch RAO are not aligned on the same frequency. This leads to smaller vessel response. The response spectrums for the system, both for vessel pitch and effective stress are shown on the following page. The pitch response (Figure 31) is notably decreased for the Gulf of Mexico environment compared with the North Sea shown in Figure 27.

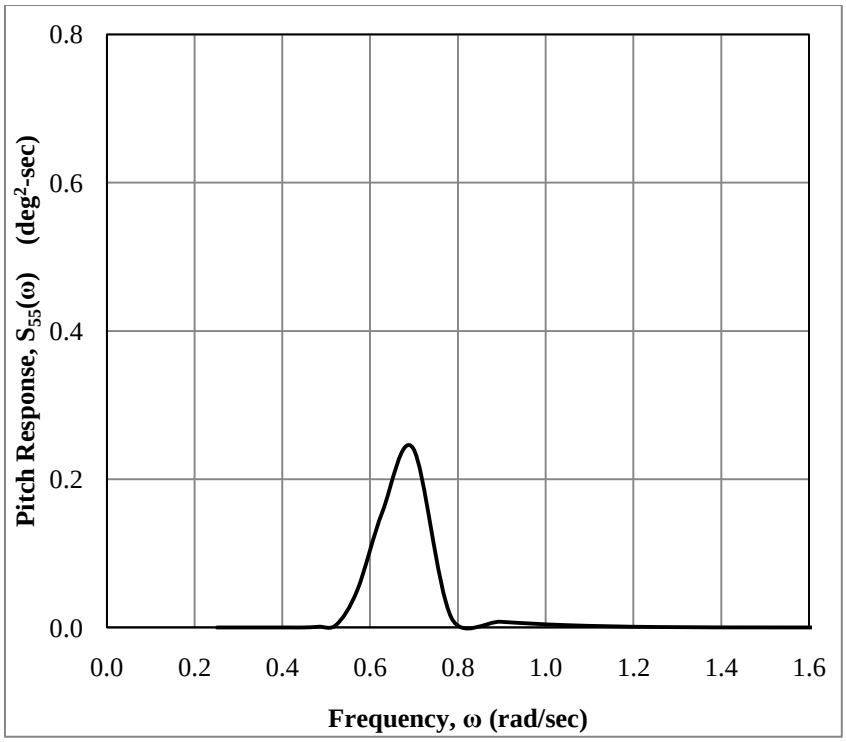

Figure 31: Pitch response spectrum, Buoy #NDBC-42055

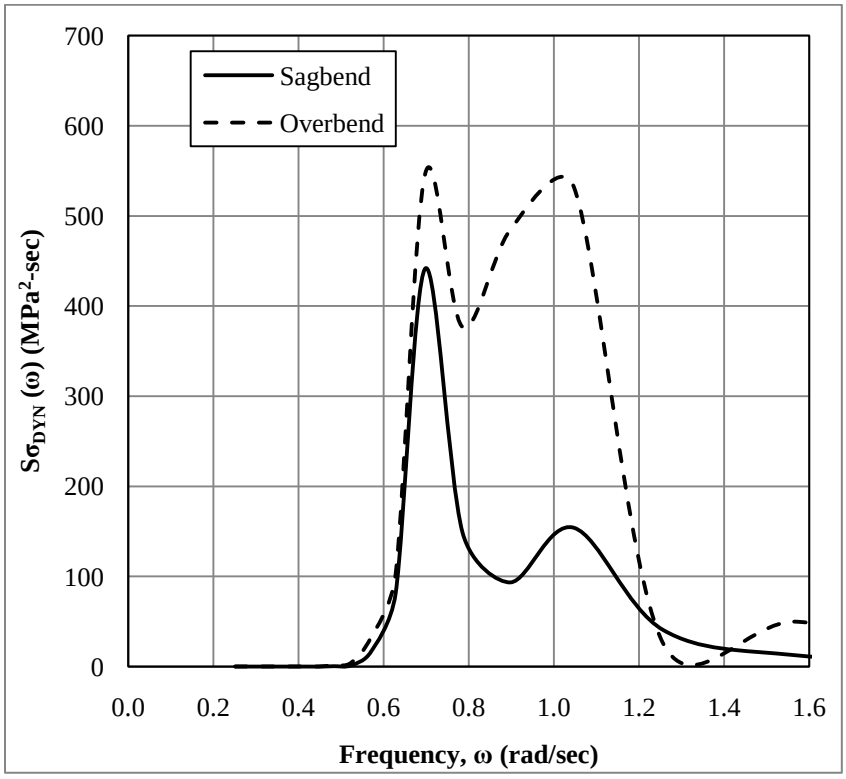

Figure 32: Dynamic stress response spectrum, Buoy #NDBC-42055

Again, the statistics of both response spectrums can be analyzed to assess the operability of the vessel.

Table 6: Statistical response properties and assessment, Buoy #NDBC-42055

Pitch (1/1000)	0.69	Deg
Allowable (1/1000)	1.50	Deg
	-54%	**Ok**
Sagbend Stress (1/50,000)	126	MPa
Sagbend Allowable (1/50,000)	390	MPa
Sagbend	**-68%**	**Ok**
Overbend Stress (1/50,000)	370	MPa
Overbend Allowable (1/50,000)	610	MPa
Overbend	**-39%**	**Ok**

Comparing the NDBC-42055 buoy's recorded sea-state against the limiting sea curves (Figure 26) the pitch and stress responses are very accurate. All three components: pitch, sagbend stress, and overbend stress, are within the allowable values as confirmed in Figure 26. The limiting sea curves are generated under the premise of a Rayleigh distribution of energy across the frequency range. While this is never fully realized in the ocean, with a long enough time sample, the spectrum will eventually take a Rayleigh shape.

Section 4 - Conclusion

As pipelines are laid in deeper water every year, improved operational limits become more critical to the success of pipelay projects. This work proposes that the use of real-time data can improve operational decision making for pipelaying vessel operators. To do so, the pipelay vessel follows a three step process. First, an adequate sample of the water surface elevation is obtained from a wave riding buoy placed by the lay-vessel. Then, a moderately trained user can adjust mooring lines, ballast water, project equipment loading, and pipe parameters to fully capture the actual vessel condition in the hydrodynamic model in *MOSES* or similar software. Finally, the recorded environment is applied to the model to obtain operational guidance as to the permissibility of pipeline stresses. By evaluating a model quickly in the frequency domain against the actual recorded sea conditions, a superintendent can make a more informed decision by considering the stresses imposed on a pipeline rather than simply stopping work if the vessel pitch limit is exceeded.

The consideration of dynamic pipeline stress should also be included in project planning workscopes as dynamic stresses can be significant and may lower the limiting sea curves used to predict the operability index, or workability, of the vessel. It was shown that at high frequencies, short periods, the pipeline may fail in bending before the vessel pitches more than 1.5 degrees. If pipeline stresses are ignored in the derivation of limiting sea curves, the pipe stresses can inadvertently be exceeded offshore in sea conditions with short periods.

An S-Lay configuration was analyzed in this work, although the method lends itself fully to other lay configurations including J-Lay. The S-Lay setup involves the added hydrodynamic effects of a stinger and requires attention be given to the overbend which is usually non-concerning in J-Lay tower systems. However, deepwater J-Lay applications may involve greater

buckling influence and additional hydrodynamic effects, such as current induced vortex shedding which has not been addressed here. For these problems, usage of CFD RANS solvers is preferred to more accurately determine the drag coefficient to apply in the hydrodynamic pipeline model. In addition, deepwater installation usually imparts a smoother stress distribution on the pipe, but creates a wider tension oscillation envelope which must be considered.

Here, industry recognized software was utilized to limit the focus to the applicability and validity of the method. Certainly, this work can be expanded to solve the dynamic pipe equations numerically and apply results from CFD analysis directly to the equations. However, the practical nature of this topic should always be forefront.

References

[1] Clauss, G. F., H. Weede, and A. Saroukh. "Nonlinear Static and Dynamic Analysis of Marine Pipelines During Laying." *Ship Technology Research* 38 (1991): 76-107.

[2] Clauss, G. F., H. Weede, and T. Riekert. "Offshore Pipe Laying Operations - Interaction of Vessel Motions and Pipeline Dynamic Stresses." *Applied Ocean Research* 14 (1992): 175-90.

[3] Clauss, G. F., A. Saroukh, and H. Weede. "Prediction of Limiting Seastates for Pipelaying Operations." *OMAE 1998-613*.

[4] Det Norske Veritas. *DNV-RP-H103 DNV Recommended Practice - Modelling and Analysis of Marine Operations*. April, 2011.

[5] Det Norske Veritas. *DNV OS-F101 Submarine Pipeline Systems*. October, 2010.

[6] Faltinsen, O. M. *Sea Loads on Ships and Offshore Structures.* Cambridge: Cambridge UP, 1998. Print.

[7] Kyriakides, S., and Edmundo Corona. *Mechanics of Offshore Pipelines*. Amsterdam: Elsevier, 2007.

[8] Lee, Jaeyoung. *Design and Installation of Deepwater Petroleum Pipelines*. Tech. 2002.

[9] Legras, Jean-Luc, and Jue Wang, Subsea 7. *Criteria for the Operation of Lowering a Structure to the Seabed Based on the Installation Vessel Motion*. OTC 21250. Offshore Technology Conference, Houston, TX, 2011.

[10] Michel, Walter H. "Sea Spectra Revisited." *Marine Technology* Winter 36.4 (1999): 211-27.

[11] Mukerji, Pabitra K. *Workability of Offshore Construction Vessels*. Tech. New Orleans, LA: McDermott, 1998.

[12] Newman, J.N., *Marine Hydrodynamics*, The MIT Press, Cambridge (1977).

[13] O'Neil, Peter V. *Advanced Engineering Mathematics*. 6th ed. Toronto: Thomson, 2007.

[14] Valen, Magnus. Launch and Recovery of ROV: Investigation of Operational Limit from DNV Recommended Practices and Time Domain Simulations in SIMO. Thesis. Norwegian University of Science and Technology, 2010.

Vita

The author was born in Kansas City, Missouri and had his focus on the field of naval architecture from the age of 12. Despite Hurricane Katrina's (2005) effects on the city, he opted to attend the University of New Orleans where he obtained his Bachelor's degree in Naval Architecture and Marine Engineering in 2010 with Departmental Honors. He participated in the university's Solar-Electric boat team for four years, winning the Sprint World Championship three times. He currently works as a Naval Architect for McDermott, Inc., a leading offshore construction company, supporting a worldwide fleet of heavy-lift and pipelay vessels.